AD-A037 740 NEW YORK UNIV WESTBURY AEROSPACE AND ENERGETICS LAB F/G 20/4
INVESTIGATION OF NOZZLE EXTERNAL FLOW.(U)
SEP 76 S PANUNZIO, A AGNONE, E TORY F33615-74-C-3071
UNCLASSIFIED AFFDL-TR-76-99 NL

1 OF 1
AD A037740

END
DATE FILMED
4-77

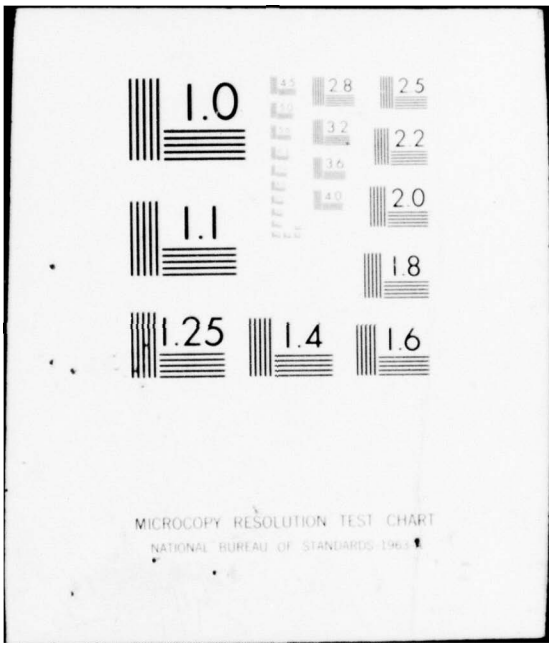
1.0
1.1
1.25
1.4
1.6
2.8
2.5
3.2
2.2
3.6
2.0
4.0
1.8
MICROCOPY RESOLUTION TEST CHART
NATIONAL BUREAU OF STANDARDS 1963

AFFDL-TR-76-99

12

ADA037740

INVESTIGATION OF NOZZLE EXTERNAL FLOW

New York University
Aerospace & Energetics Laboratory
Westbury, Long Island, New York 11590

SEPTEMBER 1976

Final Report May 1974 - October 1975

Approved for public release; distribution unlimited.

AIR FORCE FLIGHT DYNAMICS LABORATORY
AIR FORCE WRIGHT AERONAUTICAL LABORATORIES
AIR FORCE SYSTEMS COMMAND
WRIGHT-PATTERSON AIR FORCE BASE, OHIO 45433

NOTICE

When Government drawings, specifications, or other data are used for any purpose other than in connection with a definitely related Government procurement operation, the United States Government thereby incurs no responsibility nor any obligation whatsoever; and the fact that the government may have formulated, furnished, or in any way supplied the said drawings, specifications, or other data, is not to be regarded by implication or otherwise as in any manner licensing the holder or any other person or corporation, or conveying any rights or permission to manufacture, use, or sell any patented invention that may in any way be related thereto.

This report has been reviewed by the Information Office (OI) and is releasable to the National Technical Information Service (NTIS). At NTIS, it will be available to the general public, including foreign nations.

Robert C. Lock

ROBERT C. LOCK, Captain
Project Monitor
Air Force Flight Dynamics Laboratory

FOR THE COMMANDER

Alfred C. Draper

ALFRED C. DRAPER
Asst for Research & Technology
Aeromechanics Division

Copies of this report should not be returned unless return is required by security considerations, contractual obligations, or notice on a specific document.

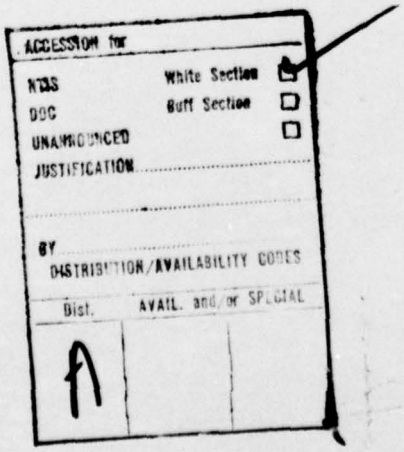

UNCLASSIFIED

SECURITY CLASSIFICATION OF THIS PAGE (When Data Entered)

REPORT DOCUMENTATION PAGE	READ INSTRUCTIONS BEFORE COMPLETING FORM
1. REPORT NUMBER: AFFDL-TR-76-99	2. GOVT ACCESSION NO. / 3. RECIPIENT'S CATALOG NUMBER
4. TITLE (and Subtitle): INVESTIGATION OF NOZZLE EXTERNAL FLOW	5. TYPE OF REPORT & PERIOD COVERED: Final - May 74 - Oct 75
	6. PERFORMING ORG. REPORT NUMBER
7. AUTHOR(s): Sergio Panunzio, Anthony Agnone and Edward Tory	8. CONTRACT OR GRANT NUMBER(s): F33615-74-C-3071
9. PERFORMING ORGANIZATION NAME AND ADDRESS: NEW YORK UNIVERSITY, AEROSPACE & ENERGETICS LABORATORY, WESTBURY, L. I., N. Y. 11590	10. PROGRAM ELEMENT, PROJECT, TASK AREA & WORK UNIT NUMBERS: 1929-04-15 / 64745F
11. CONTROLLING OFFICE NAME AND ADDRESS: AIR FORCE FLIGHT DYNAMICS LABORATORY (AFSC), AERODYNAMICS DIVISION (FXM), WRIGHT-PATTERSON AFB, OHIO 45433	12. REPORT DATE: September 1976
	13. NUMBER OF PAGES: 74
14. MONITORING AGENCY NAME & ADDRESS (if different from Controlling Office): Final rept. 15 May 74 - 31 Oct 75	15. SECURITY CLASS. (of this report): UNCLASSIFIED
	15a. DECLASSIFICATION/DOWNGRADING SCHEDULE

16. DISTRIBUTION STATEMENT (of this Report)

Approved for public release; distribution unlimited.

88p.

17. DISTRIBUTION STATEMENT (of the abstract entered in Block 20, if different from Report)

18. SUPPLEMENTARY NOTES

19. KEY WORDS (Continue on reverse side if necessary and identify by block number)

transonic tunnel, boat-tail jet plume interaction

20. ABSTRACT (Continue on reverse side if necessary and identify by block number)

The results of an experimental investigation of the transonic flow over a turbojet boat-tail including the effects of the nozzle exhaust flow are presented. A new type of transonic facility with controllable injection and porosity at the tunnel wall was developed. It was used in the present investigation to simulate accurately both the inviscid and viscous flow fields so as to best represent the complex interaction prevalent at these conditions. The operation and performance of the facility is described here.

DD FORM 1 JAN 73 1473 EDITION OF 1 NOV 65 IS OBSOLETE

UNCLASSIFIED

SECURITY CLASSIFICATION OF THIS PAGE (When Data Entered)

409427

LB

The AGARD 15° boat-tail nozzle was used in the present study since the flow field over this nacelle has been reported extensively by several investigators. Therefore it established a reference configuration that serves to check proper facility operation and for comparison of the results.

The present tests were conducted at a Mach number of approximately M_∞ .90 in a test section of 23.25 inch (59.0 cm) diameter. The unit Reynolds number was varied between 2.5 to 5×10^6 per foot. The nacelle has a 14 inch (35.5 cm) maximum diameter so that the blockage ratio ($A_{model}/A_{test\ section}$) was approximately 36%. The Reynolds number based on the nacelle maximum diameter (Re_D) was of the same order as the unit Reynolds number. In the absence of injection, the displacement thickness of the external boundary layer was approximately 1% of the nacelle maximum diameter. Injection in the boundary layer upstream of the boat-tail reduced the displacement thickness up to a factor of two. For a turbulent boundary layer, this is equivalent to an increase in Reynolds number by a factor of 32 corresponding to $Re_D \approx 1.5 \times 10^8$. These conditions exceed previous test conditions by almost two orders of magnitude. The present tests were conducted with a nozzle pressure ratio around the ideally expanded jet condition.

Detailed measurements of the static pressure distribution on the boat-tail in the facility indicate a significant upstream movement of the separation point and shock with small to moderate changes in the nozzle pressure ratio while increases in the Reynolds number cause a downstream movement of the separation point and of the shock wave.

PREFACE

This final report was prepared by Dr. Sergio Panunzio, Dr. Anthony Agnone, and Mr. Edward Tory, under the direction of Dr. Antonio Ferri, Director of the New York University Aerospace and Energetics Laboratory.

This report presents research conducted from May 15, 1974 through October 31, 1975 under Contract F33615-74-C-3071, Project No. 1921 entitled "Investigation of External Flows in Nozzles." This contract was technically monitored by Capt. Robert C. Lock and Dr. George K. Richey, Air Force Flight Dynamics Laboratory (AFSC), Wright-Patterson AFB, Ohio 45433.

The interpretation and conclusions of the data in this report are those of the authors and do not necessarily imply concurrence by the Air Force Flight Dynamics Laboratory. They are presented for the exchange of information.

TABLE OF CONTENTS

TABLE OF CONTENTS CONT'D

LIST OF ILLUSTRATIONS

LIST OF ILLUSTRATIONS CONT'D

LIST OF ILLUSTRATIONS CONT'D

LIST OF SYMBOLS

A_T	tunnel area (ft^2)
A_2	throat area at plug valve (ft^2)
A_i^*	nozzle jet exit area (ft^2)
A_j	boundary layer injection flow area
Cp	pressure coefficient
Cp_{ch}	pressure coefficient in plenum chamber
Cp_B	pressure coefficient at model wall
$Cp_T = Cp_w$	pressure coefficient at tunnel wall
Cp_D	pressure coefficient at point D (reference)
Cp^*	pressure coefficient at sonic conditions
Cp_∞	pressure coefficient at free flight reference condition
Cp_{min}	minimum pressure coefficient
D_{max}	maximum boat-tail diameter = 14 inches
M	Mach number
M_D	Mach number at point D (reference) $\cong M_\infty$
M_i	jet Mach number
M_∞	Mach number at free flight reference conditions
NPR	nozzle pressure ratio P_{oi}/p_D
$\dot{m}_i$	mass flow of nozzle jet (lbm/sec)
$\dot{m}_e$	mass flow of external flow (lbm/sec)
$\dot{m}_{jch}$	mass flow rate injected in plenum chamber (lbm/sec)
$\dot{m}_{jt}$	mass flow rate injected tangentially in boundary layer (lbm/sec)

$\dot{m}_{jn}$	mass flow rate injected normal to boundary layer (lbm/sec)
$\dot{m}_{jw}$	mass flow injected in tunnel porous wall (Fig. 3)
Poe	stagnation pressure external flow (psia)
Poi = Poj	stagnation pressure internal flow (psia)
p_D	static pressure, reference - point D (psia) (Fig. 2)
P_∞	static pressure at infinity (psia) (ideal free flight conditions)
Re	unit Reynolds number
Re_D	Reynolds number referenced to model maximum diameter
Re_{δ^*}	Reynolds number reference to δ^*
Re_x'	unit Reynolds number (ft^{-1})
R_T	radius of tunnel (ft)
R_{me}	external radius of model (Fig. 4)
R_{mi}	internal radius of model (Fig. 4)
u	axial velocity component
u_e	velocity at the edge of the boundary layer at the rake station
u_j	injection velocity of fluid into boundary layer
u/u_e	velocity ratio in boundary layer at the rake station
v_j	normal component of velocity of injected fluid
v_r/u_e	streamline slope or nondimensional radial velocity
x/D_{max}	nondimensional abscissa from model jet exit plane (Fig. 2)
$X_{Cp_{min}}/D_{max}$	axial location of Cp_{min} point on the boat-tail
X_{Cp^*}/D_{max}	axial location of Cp^* point on boat-tail
y	radial coordinate from boat-tail surface

LIST OF SYMBOLS CONT'D

y_j	jet injection slot height
δ^*	displacement thickness of boundary layer (ft)
θ	momentum thickness of boundary layer (ft)
λ	ratio of specific mass or injection parameter $\rho_j u_j / \rho_e u_e$
ρ_j	density of injected (lbm/sec ft^2) fluid
ρ_e	density of external flow (lbm/sec ft^2)
φ	meridional angle (φ = 0 at top measured clockwise looking upstream)

SECTION I

INTRODUCTION

Tactical aircraft spend an ever increasing large fraction of flight time at transonic speeds. Also subsonic aircraft must cruise at flight speeds close to the drag divergence Mach number to reduce the total flight time. At these conditions, a large percentage of the total engine nacelle drag is produced by the nozzle boat-tail. The high external drag of this region is related to the engine design. Because of the low Mach number of the flow leaving the turbine and its annular design, the turbine diameter is much larger than the minimum nozzle area where the flow is sonic. Also to minimize heating and engine weight, the area reduction is achieved very rapidly in a converging section at the rear of the engine, i.e., the boat-tail.

For a typical turbojet powered aircraft, this internal area reduction is on the order of 2.5. This rapid convergence tends to produce rapid local over expansion, in the external flow, followed by flow recompressions that produce shock waves. Usually the low momentum fluid in the boundary layer on this external surface does not negotiate the adverse pressure gradient produced by the shock-recompression system. Depending on the pressure rise produced by the shock and that associated with the subsonic pressure recovery, the boundary layer separates and forms either a separation bubble or a wake-like region. The separation is further aggravated by an additional pressure rise that is produced by the under-expanded jet plume. Since the boundary layer cannot tolerate pressure

jumps, it spreads the disturbance so as to make the pressure rise gradual. A schematic of the flow field produced by this complex interaction phenomenon is shown in Figs. 1a and 1b for the two separation modes. It is evident from Fig. 1 that the flow does not transition smoothly from one configuration to the other, since as soon as the two separation zones shown in Fig. 1a, merge, a conflict in the flow directions at the point of contact of the separation bubbles exists which cannot be reconciled by any steady flow device. A qualitative description of the flow field structure is given in Refs. 1 and 2.

Due to the nature of transonic flow, the inviscid flow field is very sensitive to the equivalent body shape that is produced by the displacement effects of the boundary layer, the flow separation, and jet plume boundary. In particular, the pressure distribution on the boat-tail can be shown (Ref. 2) to be affected by the shape of the dividing or separation streamline and by the shear forces acting on the separation zone. Therefore an accurate analytical description of this flow field must necessarily consider the coupling between the inviscid and viscous flow fields. Analytical tools to describe this flow field are presently being developed, e.g., Refs. 2-6. The modeling, however, requires as input flow properties not easily amenable to description. For example, an accurate representation of the eddy viscosity requires a knowledge of the turbulence produced by the fluctuations of the shock, separation point movement, and separation zone size and their sensitivity to free stream turbulence, external and internal flow properties, boundary layer properties, body geometry and flow asymmetries. Furthermore the understanding of this flow

field is hindered by the inability in transonic testing to simulate the pertinent similarity parameters and by wall interference effects.

To assist the theoretical modeling of this flow field, and to determine the influence of various parameters on this flow field, a special transonic facility was developed at New York University. This facility is described in Ref. 1. It is shown in Fig. 2. The external flow around the boat-tail is simulated by bounding it from below with the actual body and from above with a cylindrical surface, i.e., the tunnel wall. To alter the upper surface boundary conditions, distributed injection is used in the porous region of the tunnel wall so as to reproduce the actual streamline. This streamline is determined analytically as described in Section III B.

The internal flow is simulated mainly by using the correct jet flow Mach number and pressure ratio. For complete simulation , Ref. 2 indicates that the ratio ($\lambda = \rho_j u_j / \rho_\infty u_\infty$) of the mass fluxes per unit area of the internal flow to that of the external flow must also be reproduced. Representative initial velocity and temperature profiles and turbulence level are also necessary to insure the correct shear distribution along the dividing streamlines and the discriminating streamline (because of the normal shift), Ref. 6, of the separation zone. The viscous flow is simulated by the proper ratio of the momentum defect in the boundary layer approaching the interaction zone to a typical geometrical scale (θ/D_{max}) and not by the Reynolds number per se. This simulation is achieved in the present facility by injection (or suction) in the boundary layer on the boat-tail upstream of the interaction zone

and by changes in the unit Reynolds number through a change in the facility external flow stagnation pressure.

Flow simulation of actual configurations would also require the correct representation of such things as residual swirl, secondary nozzle coolant flow, external flow upwash hot jet effects, and other flow asymmetries in the jet, for example, due to nacelle angle of attack reflected waves from wings or adjacent engine interference phenomena. These additional parameters can best be simulated with the present technique by shrouding an actual engine.

In the present investigation, an AEDC 15^{o} boat-tail configuration was used since the flow field over this nacelle has been reported extensively by several investigators, Ref. 7. Hence it serves to check proper facility operation and for comparison of the data with other values of the flow parameters. The objective of the present investigation is to determine the influence of the boundary layer momentum thickness, nozzle pressure ratio, and variable external boundary conditions on the boat-tail pressure distribution and separation point.

SECTION II

FACILITY DESCRIPTION, CHARACTERISTICS AND OPERATION, NACELLE MODEL AND INSTRUMENTATION

A. CONCEPT

The facility design is based on the following approach. An axially symmetric tunnel and a co-axially symmetric ducted model as shown in Fig. 2 are used. The flow is divided into two streams; the stream entering the duct of the model represents the jet flow while the flow between the model and the tunnel represents the flow over the nacelle (boat-tail). The transonic test section is slotted as shown in Fig. 2. High Reynolds numbers are obtained by using a large model which gives a model to tunnel blockage ratio A_{model}/A_{tunnel} of .36.* In some cases the supersonic zone around the model extends up to the slotted tunnel wall.

The concept of the slotted wall tunnel is to tune the slots to reproduce the pressure distribution in the regions of interest (in particular on the boat-tail and on the slotted wall) and the boat-tail boundary layer characteristics. This may be achieved as follows. Suppose the flow field around a reference configuration is to be represented. Given the nacelle pressure distribution for this reference configuration, an analytical

---

* The large model also allows probing of the separation zone flow details with minimum probe interference effects.

computer program developed in Ref. 8 is used to determine the external inviscid flow field characteristics in the absence of tunnel walls. This flow field is then used to give the pressure distribution and radial velocity on a cylindrical surface corresponding to the tunnel wall. The tunnel wall porosity, the porous wall plenum chamber pressure and the distributed injection in the porous wall region are then regulated until these distributions are nearly matched. The accuracy and uniqueness of the theoretical solutions are established by comparing the theoretical pressure distribution on the tunnel wall corresponding to that of the nacelle reference pressure distribution. This tunnel wall is assumed to be far removed from the model so that interference effects are minimum.

Injection in the boundary layer upstream of the model is used to alter the characteristics (δ^*, θ) of the boundary layer approaching the interaction zone on the boat-tail. The various controls for establishing and regulating the flow are shown schematically in Fig. 3. The control mechanisms are:

1) The plug valve which changes A_2^* to establish an average upstream free stream Mach number.
2) Plenum chamber pressure control valves to regulate the pressure in the plenum chamber and the radial mass flow through the porous wall and permit communication of the upstream flow with the downstream flow so as to equilibrate the pressure.
3) Injection through the downstream region of the porous wall - affects mainly the downstream pressure, $P_{-\infty}$.

4) Porosity distribution to regulate the local mass injection.

5) Boundary layer injection - to alter the boundary layer properties.

B. DESCRIPTION AND MODIFICATIONS

The basic facility is described in detail in Ref. 1. It consists of a blowdown tunnel with a 23.25 inch (59 cm) diameter test section with a 48" long slotted wall. The modifications introduced to obtain the above flow controls and to establish the internal jet flow are discussed next.

1) The first modification was made to establish the internal flow in the nozzle model and control the NPR = P_{T_j}/p_∞. The upstream end of the model support was connected, as shown in Fig. 2, through two perforated plates to a central pipe running along the tunnel axis and entering the tunnel wall upstream of the first screen. This pipe is connected through a pressure control valve to vary the NPR. This flow is fed from an independent high pressure air bank.

2) The injection system in the boundary layer upstream of the model was modified to introduce controls for normal injection in the upstream ring and tangential injection in the middle ring, with independent air feed lines inside the annular cavity of the model through one of the three hollow legs of the model

support. The downstream injection ring was used for boundary layer suction. It was connected with the model annular cavity and the cavity itself was connected through one of the hollow legs to a duct leading through a valve to the vacuum sphere. The last capability has not been used in the present experiments.

3) The straight part of the tunnel upstream of the model was extended 12 inches to increase the zone of the porous wall test section exposed to the flow field around the jet plume up to two diameters downstream of the nozzle exit plane. The model was located with the zone of interest in the first half of the test section so that the slotted wall plenum pressure was in equilibrium to both the downstream and upstream static pressure. The static pressure at the tap location indicated by "D" in Fig. 2, was assumed to be the free stream static pressure level since this is located just upstream of the boat-tail and of the porous wall. The free stream Mach number was calculated from this static pressure and the tunnel stagnation pressure. The boundary layer pitot rake was also used as a check.

4) The downstream end of the tunnel was modified to permit exhausting the air directly into the atmosphere*. A 5° divergent diffuser** was introduced to permit operation at a test static pressure below atmospheric.

5) The mixing of the external and internal jet flow in a constant area section produces a mixed flow with a stagnation pressure that varies with the NPR. The critical area associated with the mixed flow depends therefore on the NPR. Since the plug valve was originally sized for the no internal flow condition, it permits an 11% reduction in flow area. This was found to be inadequate in regulating the downstream pressure when the converging section was removed. Therefore two injection systems were installed into the facility to be able to regulare the slotted wall plenum chamber pressure and the downstream pressure recovery. The first was achieved by admitting atmospheric air into the slotted wall plenum chamber.

---

* A tunnel stagnation pressure of 30 psia was required to be able to do so. This was attempted; however, a control valve in the system was found to be too small to pass the corresponding mass flow (~ 200 lbm/sec)

** A convergent-divergent diffuser with a 20" diameter throat was used initially in the first 30 tests. This produced a back pressure above the desired level of static pressure and rendered the plug valve ineffective in controlling the flow. Therefore the convergent section was eliminated. It is indicated in phantom lines in Fig. 2.

The flow rate was regulated by four 2.5" valves. The second was achieved by injecting approximately 3 lbm/sec* of air at the downstream end of the slotted wall. This mass addition compensates for the difference between the blockage area and the jet plume area.

C. MODEL OF AGARD 15° BOAT-TAIL GEOMETRY AND INSTRUMENTATION

The model of the AGARD 15° nozzle was fabricated in three elements: an outer and inner shell from two aluminum castings and the lip. After assembling the three parts and machining the support junction, the outer and inner contours were machined according to the profile values given in Table I. The nozzle lip was made from a stainless steel ring to obtain a good finished surface, a sharp lip, and to permit perforation of the three rings of pressure taps near the lip. The present model has a larger diameter than the versions of this model tested in the AGARD study, Ref. 7.

The pressure taps were perforated at 90° to the surface, with the annulus between the two shells used to connect the stainless steel tubing system leading the pressure taps connection out of the tunnel through one of the three supporting legs.

A total of 90 static pressure taps were installed on the model according to Table II. Of these, 54 were installed on the external surface

---

* The mass flow injected was measured with a venturi flow meter installed in the injection line.

of the boat-tail, 14 on the internal surface (to measure the jet internal flow), and 22 static pressure taps were located on the tunnel wall as shown in Fig. 2. Also, 4 static pressure taps were installed in the straight region of the non-porous tunnel wall in the $\varphi = 180^{o}$ meridional plane and 4 in the $\varphi = 0^{o}$ meridional planes. These were used to check flow asymmetries. The pressure at the location indicated by D in Fig. 2 was used as the reference pressure.

The pressure in the plenum chamber of the slotted wall was monitored by two static pressure taps at both ends of the chamber as shown in Fig. 2. A pitot dynamic probe was installed on the axis of the jet flow at $x/D = 1.60$. This was used to determine the NPR and the jet flow rate. A pitot rake with ten (10) total pressure heads and one static pressure probe, (Fig. 4) was installed on the model at $x/D = 1.4$. This was used to determine the velocity distribution in the boundary layer approaching the boat-tail. It is located downstream of the boundary layer injection system. Therefore, the effects of this injection could be determined.

The pressure taps were connected to four multiple pressure scanners* in groups of 24. Since each scani-valve has 48 ports, two readings per cycle were obtained. Each reading covered a time interval of about 1.5 sec. The transducers used were Statham model PA 208 with a range of 0-15 psia for all taps except the stagnation pressure for which a range of 0-50 psia was used. Calibration of the transducers was performed at the beginning of each series and checked every morning before the tests.

---

* Type Scanivalve Model 48-J-9

The recording was done on two Honeywell Visicorders Model 1612 with the possibility to record 36 outputs on each one. The recorder speed was 4 in/sec.

SECTION III

NOMINAL FLOW CONDITIONS

The present tests were conducted at a nominal Mach number of $M_\infty \approx .9$ with ambient temperature air in both external and jet flows. The stagnation pressure of the main flow was varied between 8 and 15 psia to give unit Reynolds number Re'_x between 2.8 and 5.2 $ft^{-1} \times 10^6$. The Reynolds number based on the maximum nacelle diameter was of the same order. The present test conditions are compared to previous investigations in Fig. 5. The present test, without boundary layer injection, are in the same Re_D range as the subscale AEDC 40 mm model in the CFF facility. In the absence of injection the displacement thickness of the boundary layer approaching the interaction zone was approximately $\delta^*/D = 1\%$ of the nacelle maximum diameter. This is in contrast to a 1.85% of the RR* tests (Fig. 23 Ref. 7, p. I-F22). Analogous results were obtained for the ratio of the momentum thickness to maximum nacelle diameter θ/D_{max}. Injection in the boundary layer can be used to reduce the value of these parameters so as to simulate Reynolds numbers Re_D on the order of 10^8 (Ref. 2).

The nominal jet flow conditions were obtained with mass flow rates from zero to 12 lbm/sec and a jet stagnation pressure of 10 to 24 psia. The actual flow conditions are indicated in the various figures. Ambient temperature air was used in the external and internal streams and in the

---

* RR Rolls Royce

boundary layer injection system. With these conditions the internal flow is choked at the trailing edge of the boat-tail.

The exit area of the boundary layer injection slots were nominally 0.88 in^{2*}, 22.5 in^2, and 22.5 in^2 for the tangential, normal injection and suction systems respectively. The injection flow rates ranges from 0 to 0.8 lbm/sec. For the normal injection system, the injection Mach number was approximately 0 to 0.15. While for the tangential system, the slot was choked for mass flow rates greater than $\sim$ 0.2 lbm/sec.

A. REFERENCE FLOW CONFIGURATION

The reference flow field was used in the present tests corresponds to a free stream Mach number of 0.91, an NPR = 3.1, and $Re_D = 1.2 \times 10^6$. At these conditions, a significant interaction between the external and exhaust flows was expected due to the sizable supersonic zone, boundary layer thickness, and recompression pressure rise. The inviscid flow field about this configuration was obtained with the aid of a computer program described in Ref. 8. The boat-tail pressure distribution for this configuration is shown in Fig. 6a**. This represents the "mean" line of the data obtained at several facilities (Ref. 7 & 9) with nominally the same flow conditions. The shape of the dividing (separation) streamline was determined iteratively (i.e., in the first iteration the actual body radius was used to evaluate the axisymmetric terms in the governing

---

* Slot height of .020"

** The RR data was the first data available to the authors

equations, successive iterations used the calculated dividing streamline). The pressure variations along the calculation grid (shown in the lower half of Fig. 6b) used in the program are shown in the upper part of Fig. 6b. The curves are labeled according to the grid numbers.

The input body pressure distribution (Fig. 6a), the shapes of the sonic line, shock and dividing streamline are also shown. The pressure distribution on a cylindrical surface corresponding to the New York University tunnel wall was determined from this flow field calculation. It is also shown in Fig. 6b. Several streamlines in the region of interest are shown in the lower half of Fig. 6c*. The radial flow variation along the tunnel wall required to simulate free flight is shown in the upper half of Fig. 6b. The streamline asymptotic to the tunnel wall shown in the lower half of Fig. 6b is the one which must be reproduced accurately to avoid tunnel wall interference. Distributed injection, controlled by the porosity distribution and total amount of mass injected at the tunnel wall, analogous to the radial velocity distribution at the wall was used in the present investigation to simulate this streamline. Additional injection was used to insure that the measured tunnel wall pressure reproduced the theoretical distribution and that the downstream boundary condition ($P_{+\infty} = P_{-\infty}$) was satisfied. The amount of injection had to be varied for different NPR to insure that this condition was always satisfied.

---

* Note the change in flow deviation at the shock is on the order of 1.7 degrees. Also a necking of the flow appears near the body.

B. EXPERIMENTAL PROGRAM

The experimental program was divided in two phases. In the first phase, the facility operation and the reference flow configuration described above were established. The porosity distribution, amount of injection in the porous wall region and plug valve position required to match the theoretical wall pressure distribution as close as possible were determined. In this phase of the investigation, modifications 4 and 5 described above were introduced.

In the second phase, the characteristics of the boundary layer approaching the interaction region were varied by injection. The unit Reynolds number and NPR were also varied by increasing the external air stagnation pressure from 8 to 15 psia while the stagnation pressure of the jet flow was held constant. A list of runs conducted in phase one is given in Table III-A. The actual values of the flow parameters attained (Mach No., Po_e, Po_i), the wall porosity configuration, the porous wall plenum chamber pressure coefficient, and porous wall injection flow rates are given for each run. The list of runs conducted in the second phase of the program are presented in Table III-B.

The porosity distribution used in the various groups of tests is presented in Fig. 7. The porosity injection code is indicated at the bottom of the figure. A closed (0) porosity-injection code signified no injection in this section. This is achieved by closing the five holes on the perforations of the 3" wide outer strips (Ref. 1, pp. 19-20). This produces a porous cavity as in standard transonic wind tunnels. An open

(1) porosity-injection code signifies injection in the region. This is achieved by opening the same holes on the 3" wide outer strips so as to admit air from the plenum chamber of the slotted walls into these regions. The flow rate of this air depends on the difference in the plenum chamber pressure to the local wall pressure, on the curvature of the simulation streamline, and on the pressure drop produced by the strips and porous wall itself. A porosity injection code of (3) "strip out" is achieved by removing the outer perforation strip so as to eliminate the pressure drop caused by it. This would tend to increase the injection flow rate above that produced by a porosity code of (1).

A porosity injection code (2) was achieved by connecting the air injection nozzle placed in these sections to an independent air supply system as shown in Figs. 2 and 3*. It appears from the development of the porosity-injection codes presented in Fig. 7 and especially configuration F, that the injection distribution should tend towards a distribution similar to the radial velocity distribution at the tunnel wall shown in Fig. 6b.

---

* In this configuration the outer strips are in a closed position as in configuration 0. However, these sections (labeled 2 in Fig. 7) do not communicate with the porous wall plenum chamber. Hence they do not affect the porous wall plenum chamber pressure while air is injected in the test section with the 30 nozzles distributed in the porous wall.

SECTION IV

TUNNEL OPERATION & ATTAINMENT OF THE REFERENCE FLOW CONFIGURATION

The tunnel operation and the reference flow configuration described above were attained in the first phase of the program. The various controls used to regulate the test section flow (Section II A and Fig. 3) were varied until the tunnel wall pressure distribution approximated the theoretical one shown in Fig. 6b*. The intended use of this facility is to explore flow field changes produced by variations in flow parameters or initial and boundary conditions that have a "limited" zone of influence as opposed to changes that are produced by flow parameters that affect the entire flow field (e.g., Mach number and Nozzle pressure ratio). It may also be used to determine flow changed produced by perturbations in the principal flow parameters (i.e., M_∞, NPR) about a reference flow condition which is assumed given. Therefore, this type of facility does not have the disadvantages due to tunnel wall interference problems as encountered in a conventional transonic facility since conceptually the facility can be used to reproduce the initial and boundary conditions around a transonic flow region of interest.

---

* The correct boat-tail pressure distribution is also obtained when the wall pressure distribution is reproduced since the initial and other boundary conditions (e.g., nozzle exhaust plume) are simulated, if there is a "unique" solution (i.e., the flow is not extremely sensitive to the boundary and initial data).

A systematic study of the effect of each flow control separately was not possible because of the large range and combination of the parameters involved and because the changes produced by one control are coupled to that of another. Nevertheless, after a series of exploratory tests, certain trends in the flow changes produced by the different controls became apparent. A summary of the effects produced by control variations and tunnel modifications described above is presented next to define qualitatively the tunnel operation. The tunnel wall pressure distribution and the variations of the chamber pressure with various control locations will be used for this purpose.

Referring to Table III A, the first 30 tests were conducted with a converging-diverging diffuser with a minimum section diameter of 20" and the plug valve was moved forward as shown in phantom lines in Fig. 2. The first two tests were conducted without internal flow ($\dot{m}_i = 0.0$). Therefore the pressure taps on the internal surfaces and the pitot probe inside the jet flow measured the "base" pressure of the flow in this configuration. The base pressure varies between 0.6 to 0.76 of the freestream static pressure depending inversely with the free stream Reynolds number.

In the first series of tests, the NPR was varied for each of the first three porosity-injection codes (A, B, C) shown in Fig. 7. The plug valve was held fixed and the tunnel stagnation pressure, Po_e, was nominally 11 psia. The measured tunnel wall pressure distribution for these three configurations (Tests 6, 24, and 28) is shown in Fig. 8a for a NPR near 2.0 and a resulting chamber pressure coefficient near zero. The corresponding

pressure distributions on the boat-tail are shown in Fig. 8b.

Generally the wall pressure distribution for each case compares favorably with that of the reference configuration, except near the end (only when $m_{jw} = 0$) where an over-pressure is observed and upstream at $x/D > 1.6$. Nevertheless, the effect of the porosity injection, code 2, is evident from a comparison of the wall pressure distribution measured in Tests 6 and 24. The effect of the porosity-injection code B and C is evident by comparing tests 24 and 28.

The high pressure recovery downstream of the model, shown in Fig. 8a, was thought to be caused by the choking effects produced by the converging-diverging diffuser. Therefore the converging section of the diffuser was removed and the plug valve assembly was shifted back as shown in Fig. 2. An attempt to exhaust to the atmosphere was also made at this time but failed due to the inability to attain a high external flow stagnation pressure. The porosity injection configuration was also changed at this time as indicated in Table III A.

In the next sequence of tests, the influence of porosity-injection code, plug valve position, mass injection into the porous wall chamber, and NPR on the tunnel wall pressure was studied.

A. EFFECT OF PLUG VALVE POSITION

The plug valve location was varied incrementally as shown in Fig. 2 from the aft most position (8"), to the mid position (12"), to the forward most position (16"). The tunnel wall pressure distribution with these three plug valve positions is shown in Fig. 8c. The jet NPR and porosity

codes are indicated in Table III A. A significant change in the tunnel wall pressure distribution due to the end plug valve position is clearly evident. A downstream motion of the plug valve reduces the back pressure which causes the porous wall chamber pressure to drop along with the tunnel wall pressure. The corresponding pressure distributions on the boat-tail are shown in Fig. 8d. The chamber pressure and the tunnel pressure distribution on the aft end are intimately connected to the plug valve position. A correlation of the data from all tests of the plenum chamber pressure with the plug valve position is shown in Fig. 8d. The spread in the data is due to other parameters. Clearly the chamber pressure drops with downstream motion of the plug valve.

To reproduce the simulation streamline indicated in Fig. 6c, there must be injection at the porous wall, since the streamline deflects downward. This can be achieved only if the chamber pressure is greater than the maximum tunnel wall pressure indicated by the theoretical curve of the reference configuration. A chamber pressure below this level causes inflow into the chamber and a recirculation of the fluid. An allowance must also be made for the pressure drop produced by the porous screens. Analysis of the data shows that a ΔCp of approximately 0.06 is produced by the porous wall. Adding this value on the theoretical wall pressure peak of $Cp_w \approx .070$ gives a plenum chamber pressure of approximately $Cp_{ch} \approx .13$ for correct simulation. The porosity of the wall distributes the flow according to the radial velocity at the wall.

B. INFLUENCE OF NOZZLE PRESSURE RATIO (NPR)

The influence of the NPR on the plenum chamber pressure is correlated in Fig. 8f for the three plug valve positions. Generally an increase in the NPR causes an increase in the jet plume angle. This causes an increase in the back pressure that is felt in the plenum chamber pressure.

The influence of the NPR on the tunnel wall pressure distribution is shown in Fig. 8g when the plug valve is at the 12" position. A general increase in the pressure level in the rear is evident with increasing NPR. This implies an upstream movement of the shock on the boat-tail. The influence of the nozzle pressure ratio on the boat-tail pressure distribution is discussed below.

C. EFFECT OF INJECTION IN THE PLENUM CHAMBER OF POROUS WALL

The effect of mass addition in the plenum chamber of the porous wall on the tunnel wall pressure distribution is shown in Fig. 8h for two plug valve positions. The mass addition was controlled by four (4) gate valves. By varying the number of open valves and the degree to which they are open, different flow rates could be attained.

D. ATTAINMENT OF THE REFERENCE CONFIGURATION

The correlations presented above show the difficulty in fixing the exact flow conditions needed to obtain the reference flow configuration with the existing hardware. In spite of this, a flow pattern close to the reference configuration was obtained in test 58. The values of the flow parameters used to obtain this reference configuration are presented

in Table III B.

The tunnel wall pressure distribution for this configuration is shown in Fig. 9a. The reference distribution is also shown for comparison. The difference in the curves is attributable in part to the low chamber pressure in this test and in part is a misrepresentation of the plume boundary layer in the analysis of the inviscid flow field (see Section III B p. 14). The wall pressure distribution in the region following the shock was subsequently corrected during the second phase as evident from the data from tests 64 and 68 shown in Fig. 9a. The tunnel wall pressure distribution calculated assuming no separation on the boat-tail and a straight sting with a diameter equal to that of the jet exit is also shown for reference. This represents the limit case of infinite Reynolds number and an NPR of about 2.

The pressure distribution on the boat-tail is shown in Fig. 9b for test 58. The pressure variation used in the analysis, from Ref. 7 and 9 (see Section III B above), the CFF data (Ref. 7 IF 19 Fig. 15b)* taken at the highest Reynolds number, and the calculated pressure distribution for the no-separation, straight sting case, are also shown. The present data agrees with the CFF data and is bracketed by the two cases. The difference between the analyses and the data is due to the Reynolds number and NPR. These data tend to imply that an increase in the Reynolds number and a decrease in NPR cause a downstream movement of the minimum pressure point,

---

* CFF compressible flow facility at Lockheed Aircraft - Georgia

i.e., the recompression is delayed. The flow asymmetry evident* in the data can arise from 1) accuracy in the pressure measurements, 2) facility asymmetries (such as model and tunnel axis mis-alignment, porous wall slot non-uniformities, etc.), and 3) model support strut wakes that affect the boundary layer growth. The present data shows a scatter in the Cp of $|\Delta Cp| = 0.08$. A similar variation is observed in the data presented in Ref. 7 (II-E12 Fig. 15). The error in the pressure measurements is estimated to produce an error in the Cp of $\Delta Cp \approx \pm .010$. The present data also shows asymmetry in the expansion zone. This is mainly due to facility asymmetries. It is not immediately evident how much pressure asymmetry is produced by a given facility mis-alignment. A quasi-axisymmetric analysis, e.g., Ref. 10, might answer this question. A non-symmetry in the peripheral boundary layer distribution is discussed in Ref. 7 II-E with reference to the NASA data. A non-uniform boundary layer produces an asymmetric equivalent body and causes flow separation to occur at different axial stations in the different peripheral planes. This phenomenon is important in the understanding of the boat-tail flow field. Therefore further investigation in this direction is suggested.

---

* Asymmetry in the present data is mainly about vertical plane of symmetry. The data shows symmetry about a horizontal plane to within the accuracy of the present measurements.

SECTION V

DATA PRESENTATION AND ANALYSIS

Having established the basic tunnel operation and approached the reference flow configuration to the current capability of the facility, the external flow unit Reynolds number and nozzle pressure ratio ($NPR = Po_i/P_\infty$) were varied by changing the free stream stagnation pressure. Also, the characteristics (θ, δ^*) of the boundary layer approaching the boat-tail region were altered by injection. The objective of this investigation was to determine the sensitivity of the external flow (e.g., movement of the Cp^* and Cp_{min} points) to these parameters. All other flow controls were held nominally fixed in this phase (see Table III B).

A. EFFECT OF BOUNDARY LAYER INJECTION

Both normal and tangential injection modes were used to produce different boundary layer profiles and characteristics. The injection flow rate was varied between 0 and 0.8 lbm/sec in both cases.

1. Normal Injection Mode

The boundary layer profiles measured at the rake station x/D = 1.40 with different rates of mass injection are shown in Fig.10. The injection parameter $\lambda = \rho_j u_j/\rho_e u_e$ is indicated in the figure for reference. (For normal injection $\lambda = \rho_j v_j/\rho_e u_e = \frac{\dot{m}_j/A_j}{\dot{m}_\infty/A_T}$). The nozzle pressure ratio for this series of tests was nominally 3.30 and the Reynolds number based on the nacelle maximum diameter was nominally 4×10^6. The displacement effect due to normal injection is clearly evident from these profiles. The

boundary layer displacement and momentum thickness calculated from these profiles are indicated in the figure and are plotted vs the injection parameter, $\lambda = \rho_j u_j / \rho_e u_e$, in Figs. 11a and 11b respectively. The trends calculated assuming the thicknesses are the sum of the thicknesses without injection plus the defects (or excesses) due to the injection are shown for comparison. The normal injection case was treated similar to a tangential injection mode with very low injection velocity $u_j/u_e \ll 1$, and $\rho_j u_j / \rho_e u_e$ finite. In view of the ambiguity of the equivalent slot height, in this case, a family of curves with values of y_j/D that lie between that corresponding to the normal injection ($y_j/D \approx .033$) and that of the tangential one ($y_j/D \approx .00167$) are shown. The thicknesses are nearly constand for values of $\rho_j u_j / \rho_e u_e$ less than .10. The theoretical momentum (displacement) thickness increases (decreases) linearly with this parameter. The lack of a definitive trend in the experimental data is perhaps due to the complexity of the flow field associated with normal injection and to insufficient data.

2. Tangential Injection Mode

The boundary layer profiles with tangential injection are shown in Figs. 12 and 13. The values of the flow parameters are indicated in the figures. A velocity excess is evident in Fig. 13 for the case of the highest injection velocity and lowest Re_D. The velocity profiles are much fuller than those with normal injection.

The displacement and momentum thickness variation with the injection parameters are shown in Figs. 11a and 11b respectively. In this case,

both thicknesses decrease with increasing values of the injection parameter. The data exhibit the same trend as calculated by adding the thickness due to the jet and the injection values. The incremental defect due to the slot mixing is evident from a comparison of the data with the curves. The incremental defect increases with increasing values of the injection parameter. A momentum excess is evident for values of λ greater than 3 with correspondingly sizable reduction in displacement thickness.

The boat-tail pressure distribution, with boundary layer injection upstream of the interaction zone, are presented in Fig. 14 for normal injection rates so that the injection parameter is between 0.02 and 0.15. In spite of the large difference in the velocity profiles (Fig. 10) with normal injection, no consistent trend in the pressure distribution could be ascertained due to the large pressure gradients prevalent on the boat-tail, the accuracy of the data, and the rather narrow range of the momentum thickness (θ/D) parameter used in these tests. To obtain a clear indication of the trends, the momentum thickness should be increased by both reducing the injection area used in the normal injection case and increasing the injection flow rate; or by possibly injecting a light gas with diffusion characteristics similar to those of air. Also a tighter control on the plenum chamber pressure should be exercised.

The boat-tail pressure distributions with tangential injection upstream of the interaction zone are shown in Fig. 15 for values of the injection parameter $\lambda = \rho_j u_j / \rho_e u_e$ between 0.46 and 4.6. Again a definite trend of the data with increasing values the injection parameter cannot

be established. However, after correcting the data for the differences in the chamber pressure (i.e., shifting the data along the Cp ordinate) and taking only data that follow a uniform trend with variations of the momentum thickness, a tendency towards the inviscid no separation case; or equivalently high Reynolds number, can be seen. This is made more evident below when we correlate the locations of the Cp^* and Cp_{min} points.

B. EFFECT OF REYNOLDS NUMBER AND NPR

The boat-tail pressure distributions obtained by increasing the tunnel stagnation pressure from 9 to 15 psia while holding all other parameters fixed and with the maximum tangential injection flow rate of 0.8 lbm/sec are shown in Fig. 16. In this case, the injection parameter, unit Reynolds number and NPR varied because the stream static pressure changed. However a direct comparison of the effect of the unit Reynolds number only can be obtained by comparing the pressure distributions obtained in tests 58 and 73 (no injection cases). The downstream movement of the Cp_{min} point with increasing Reynolds number is evident. Unfortunately part of this change is also due to a change in NPR. A comparison of the pressure distribution shown in Fig. 16 (after correcting for the chamber pressure) show little change. This is due to the fact that while increasing the NPR tends to move the Cp_{min} point upstream, increasing the Reynolds number tends to move it downstream (see Ref. 11).

C. CORRELATIONS

In spite of the above difficulties and uncertainties, some correlations of the characteristics of the flow field structure were attempted. The

locations of the Cp_{min} and the downstream Cp^* were correlated with the unit Reynolds number Re_D, NPR, and θ_o/δ^*_o. The Cp_{min} point gives some indication of the separation point while the Cp^* gives an indication of the shock location. The location of the Cp_{min} point is correlated in Figs. 17a, 17b, and 17c with the Reynolds number Re_D, NPR and θ_o/δ^*_o respectively. These correlations show the following trends:

1) The Cp_{min} point moves downstream, $(x/D)_{min}$ decreases with increasing values of Re_D. The scatter in the data is due to different NPR and Re_D and in the accuracy of locating the Cp_{min} point from the data.
2) The Cp_{min} point moves upstream with increasing nozzle pressure ratio. The trend is more clearly defined in the case of tangential injection than the case of normal injection.
3) The correlation of the Cp_{min} point with the momentum thickness at the start of the interaction zone, θ_o, shows a decreasing trend. Additional analysis of the data is required to remove the influences of the NPR and Re_D.

The correlation of the downstream Cp^* point with Reynolds number Re_D is shown in Fig. 18a. This shows that the Cp^* point moves downstream with increasing values of Re_D. The movement of the Cp^* point is greater than that of the Cp_{min} point. Therefore the distance between these points increases with increasing Re_D. The dependence of the Cp^* point on the NPR is shown in Fig. 18b. This shows a clearly defined

trend which is mainly due to the increased back pressure produced by a larger plume with increased NPR.

SECTION VI

SUMMARY, COMMENTS & RECOMMENDATIONS

A new type of transonic wind tunnel facility that uses a shrouding technique is described here. The operation and characteristics of this facility have been defined in terms of the various flow controls necessary to produce a desired flow field. Some facility and control improvements are indicated from the present results to simulate more accurately the flow field and to extend the capabilities of this facility.

The facility has been used here to reproduce the transonic flow field over the boat-tail of a turbojet nacelle including the effects of the jet exhaust flow plume. A reference flow configuration (M_∞ = .9, NPR = 3.0, and $Re_D = 1.2 \times 10^6$) was tentatively established. Then the effects of variations in NPR, Re_D, and the boat-tail initial boundary layer characteristics (δ^*, θ) on the boat-tail pressure distribution were investigated. Injection in the boundary layer approaching the interaction region was used to alter its characteristics (δ^*, θ).

Tentative correlations of the minimum pressure and the downstream sonic point on the boat-tail with these parameters, indicate a downstream movement of these points with increasing Re_D and decreasing NPR. The influence of the boundary layer injection on these points is less clearly defined probably because the values of the injection parameters were not varied to sufficiently alter the boundary layer characteristics.

The results presented here can be correlated more accurately for the present configuration if the individual effects of each parameter can be established quantitatively. This can be achieved semi-empirically by

using the present data and the analysis presented in Ref. 8 with correction for the boundary layer growth on the boat-tail and refined estimates of the plume shape. These analyses should be conducted for a range of the pertinent parameters extending over at least one order of magnitude beyond the present tests.

The analyses can be further refined if the details of the structure of the separation bubbles are included in the theory. The present facility is most suited for this purpose since due to the large model size, the separation zone has sizable dimensions hence probe interference effects can be minimized. Also additional experiments should be conducted at free stream Mach number near unity when the influences of the individual parameters are more pronounced. A capability exists presently to simulate a hot jet with $T_o = 1200^{\circ}R$ and the throat cooling. In this connection, the jet exhaust flow profiles can be measured to define rigorously the initial data. The plume boundary, jet boundary layer, and heat transfer rates at the nacelle wall can be determined accurately. Values of the injection parameter greater than 5 should be used to obtain a significant influence of the injection on the flow field.

TABLE I ORDINATES OF 15° AGARD NOZZLE GEOMETRY

EXTERNAL				INTERNAL	
X/D	Y/D	X/D	Y/D	X/D	Y/D
0	0.2075	0.700	0.4490	0	.407
0.025	0.2155	0.725	0.4543	.179	.451
0.050	0.2245	0.750	0.4595	.516	.627
0.075	0.2349	0.775	0.4645	1.014	.686
0.100	0.2458	0.800	0.4695	1.124	.731
0.125	0.2568	0.825	0.4743		
0.150	0.2678	0.850	0.4788		
0.175	0.2788	0.875	0.4828		
0.200	0.2888	0.900	0.4863		
0.225	0.2988	0.925	0.4898		
0.250	0.3085	0.950	0.4928		
0.275	0.3180	0.975	0.4953		
0.300	0.3275	1.000	0.4978		
0.325	0.3368	1.025	0.4990		
0.350	0.3458	1.050	0.5000		
0.375	0.3545	3.000	0.5000		
0.400	0.3630				
0.425	0.3718				
0.450	0.3800				
0.474	0.3880				
0.500	0.3958				
0.525	0.4033				
0.550	0.4108				
0.575	0.4178				
0.600	0.4248				
0.625	0.4313				
0.650	0.4375				
0.675	0.4435				

TABLE II EXTERNAL STATIC PRESSURE INSTRUMENTATION

X/D	ϕ (ANGULAR ORIENTATION)					
	0	45	90	135	180	270
.035	X	X	X	X	X	X
.075	X		X		X	X
.135	X	X	X	X	X	X
.195	X		X		X	X
.285	X	X	X	X	X	X
.395	X		X		X	X
.505	X		X		X	X
.625	X	X	X	X	X	X
.725	X		X		X	X
.825	X				X	
.995	X				X	
1.175	X		X		X	X
1.425	X				X	
1.805	X		X		X	X
2.545	X		X			
3.015	X		X		X	
4.275	X				X	
5.385	X				X	
7.715	X				X	
8.035	x					
9.245	X					
10.515	X					
11.725	X					
13.205	X		X		X	X

TABLE III-A PARAMETRIC REPRESENTATION OF ALL TESTS

TEST #	MACH #	$P_{o\ Ext}$	$P_{o\ Int.}$	WALL CONFIG.	N.P.R.	Cp_{ch}	$\dot{m}_{jw}$ CODE 2
1	.83	13.0	4.6	A		-	-
2	.86	9.0	4.1	A		-	-
3	.88	12.0	15.0	A	2.58	.156	-
4	.94	11.5	17.0	A	2.88	-.164	-
5	.95	12.0	15.0	A	2.20	-.186	-
6	.86	12.0	13.0	A	1.94	0.0	-
7	.94	11.0	7.0	A	1.06	-.269	-
8	.93	12.0	5.0	A	0.79	-.367	-
9	.86	11.2	14.6	A	2.11	.165	-
10	-	-	-	A	-	-	-
11	-	-	-	A	-	-	-
12	-	-	-	A	-	-	-
13	.84	12.0	18.0	A	2.57	0.0	-
14	-	-	-	A	-	-	-
15	.92	11.0	12.4	A	1.84	.087	-
16	.92	10.5	8.0	A	1.27	-.158	-

TABLE III-A PARAMETRIC REPRESENTATION OF ALL TESTS CONT'D

TEST #	MACH #	$P_{o\ Ext}$	$P_{o\ Int.}$	WALL CONFIG.	N.P.R.	Cp_{ch}	$\dot{m}_{jw}$ CODE 2	
17	.93	11.0	17.0	A	2.52	.024	0.0	Introduce injection through Stations 12 - 16 m_j Code 2
18	.89	11.0	12.8	B	1.83	-.205	.35	
19	.89	9.75	13.0	B	2.09	-.116	.36	
20	.89	10.5	12.1	B	1.86	-.125	1.50	
21	.89	11.0	14.8	B	2.16	-.052	2.6	
22	.89	11.0	13.9	B	2.00	-.195	3.0	
23	.87	11.0	17.2	B	2.44	-.053	3.0	
24	.87	10.0	13.9	B	2.14	-.058	3.0	
25	.89	9.0	12.0	C	2.14	-	3.0	
26	-	-	-	C	-	-	-	
27	.86	10.0	13.9	C	2.06	.014	3.0	
28	.87	10.0	13.8	C	2.06	.010	3.0	
29	.81	10.0	13.7	C	2.03	.016	3.0	Sealed plenum valve introduce injection into plenum chamber
30	.79	10.0	14.3	C	1.99	.032	3.0	
31	.83	9.8	13.0	C	2.09	.075	3.0	
32	-	-	-	C	-	-	-	
33	.87	10.5	10.8	C	1.56	.027	3.0	

TABLE III-A PARAMETRIC REPRESENTATION OF ALL TESTS CONT'D

TEST #	MACH #	P_o Ext	P_o Int.	WALL CONFIG	N.P.R.	Cp_{ch}	$\dot{m}_{jw}$ CODE 2	
34	-	-	-	D	-	-	-	EJECT TO ATMOSPHERE
35	-	15.5	-	D	-	-	-	
36	.51	15.3	-	D	-	-	-	
37	.61	15.8	-	D	-	-	-	
38	.56	15.6	-	D	-	-	-	
39	.78	16.7	12.5	D	1.13	-	-	
40	.89	10.7	9.4	D	1.47	-.761	0.0	PARTITIONS INTRODUCED IN SLOTTED WALL
41	.90	11.3	12.9	D	1.92	-.342	2.1	
42	.90	11.0	13.0	E	2.00	-.347	2.1	
43	-	-	-	E	-	-	-	
44	.87	11.0	14.0	E	2.09	-.111	2.4	
45	.88	11.0	13.4	E	2.03	0.0	3.0	
46	.85	10.8	13.9	E	2.07	.088	3.0	
47	.86	9.6	13.0	E	2.16	.161	3.0	
48	.90	10.5	12.9	E	2.06	.084	3.0	
49	.89	10.4	13.1	E	2.09	0.0	3.0	
50	.99	11.6	13.7	E	2.24	0.0	3.0	

TABLE III-A PARAMETRIC REPRESENTATION OF ALL TESTS CONT'D

TEST #	MACH #	$P_{o\ Ext}$	$P_{o\ Int.}$	WALL CONFIG	N.P.R.	$C_{p_{ch}}$	$\dot{m}_{jw}$ CODE 2
51	-	-	-	F	-	0.0	-
52	-	-	-	F	-	-	-
53	.89	9.7	10.7	F	1.86	.060	3.0
54	.88	8.8	10.8	F	2.04	0.0	1.6
55	.86	8.9	14.2	F	2.58	.175	3.0
56	.88	10.6	21.5	F	3.36	-.029	3.0
57	.89	9.9	17.3	F	2.93	-.288	3.0

TABLE III-B PARAMETRIC REPRESENTATION OF ALL TESTS CONT'D

TEST #	MACH #	$P_{o\ Ext}$	$P_{o\ Int}$	CONFIG.	N.P.R.	Cp_{ch}	$\dot{m}_{jw}$ CODE 2	$\dot{m}_{BL}$
58	.88	9.4	19.3	F	3.38	0.0	3.0	0.0
59	.89	10.0	20.3	F	3.38	-.691	3.0	.1N
60	.92	10.5	19.0	F	3.11	-.055	3.0	.2N
61	.88	9.9	19.8	F	3.30	.061	3.0	.4N
62	.88	10.3	19.0	F	3.04	-.074	3.0	.8N
63	.89	10.7	19.0	F	2.99	-.084	3.0	.15N
64	.89	9.4	19.5	F	3.45	.112	3.0	.25N
65	.89	10.8	19.6	F	3.04	-.070	3.0	.1T
66	.88	9.1	20.1	F	3.65	0.0	3.0	.2T
67	.90	10.4	23.3	F	3.82	.260	3.0	.4T
68	.83	8.8	23.0	F	4.10	.148	3.0	.8T
69	.87	10.8	23.3	F	3.53	.057	3.0	.8T
70	.88	11.7	23.0	F	3.26	.065	3.0	.8T
71	.90	13.4	22.8	F	2.88	-.156	3.0	.8T
72	.90	14.7	23.6	F	2.71	-.162	3.0	.8T
73	.90	14.7	24.6	F	2.83	-.182	3.0	0.0

PROPER TUNNEL AND FLOW CHARACTERISTICS OBTAINED AND BOUNDARY LAYER CONTROL INTRODUCED

TABLE III-B PARAMETRIC REPRESENTATION OF ALL TESTS CONT'D

NOTE:

1) Reference Mach number was taken at point D at the end of the wall straight section, upstream of the model

2) Injection from the atmosphere into the chamber at 6 psia (avg) from Test 30-46 $\dot{m}_{ch}$ (avg) 3 lbm/sec and from tests 47-73 $\dot{m}_{ch}$ (avg) 6 lbm/sec.

3) Plug valve at tunnel exit positioned at 12" for tests 58-73

4) Plenum chamber valve to exhaust manifold system was sealed from tests 29-73 to avoid pressure feedback

5) Partition introduced into the slotted wall from tests 40-73 to minimize circulation of the flow in the slots

6) Tunnel cross section at the end plug valve was opened up to the full test section diameter from tests 40-73

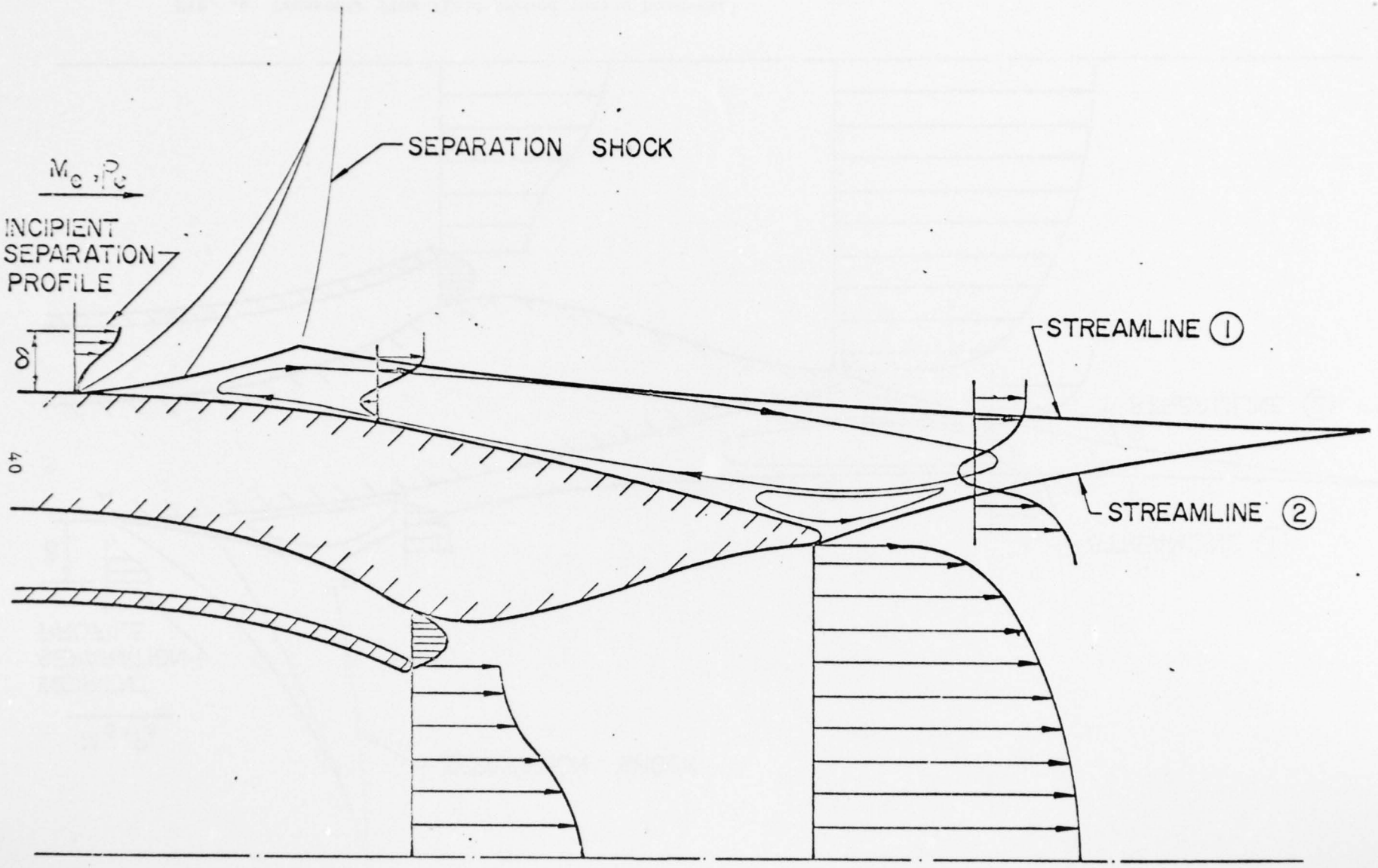

Fig. 1a Transonic flow field around nozzle boat-tail

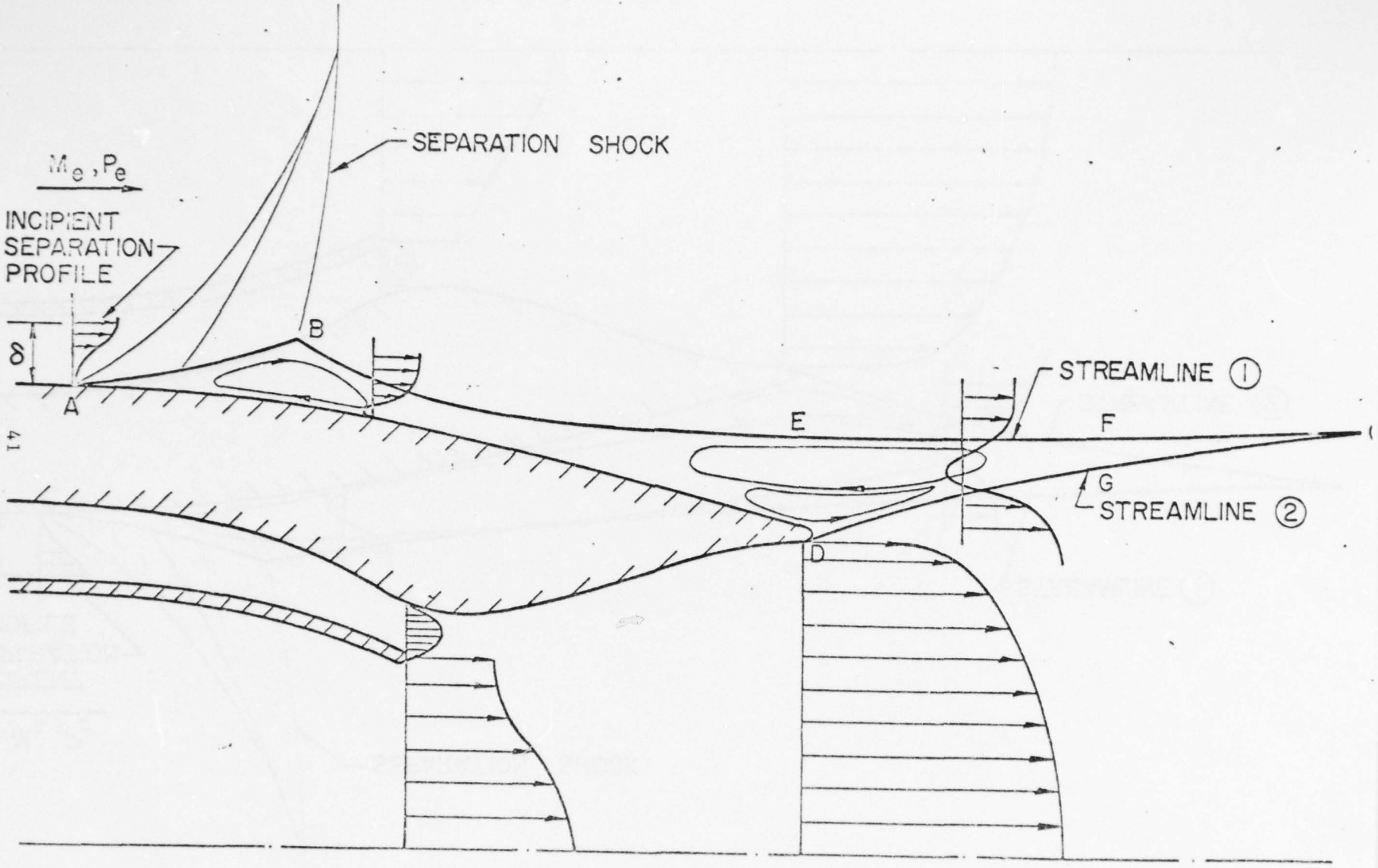

Fig. 1b Transonic flow field around nozzle boat-tail

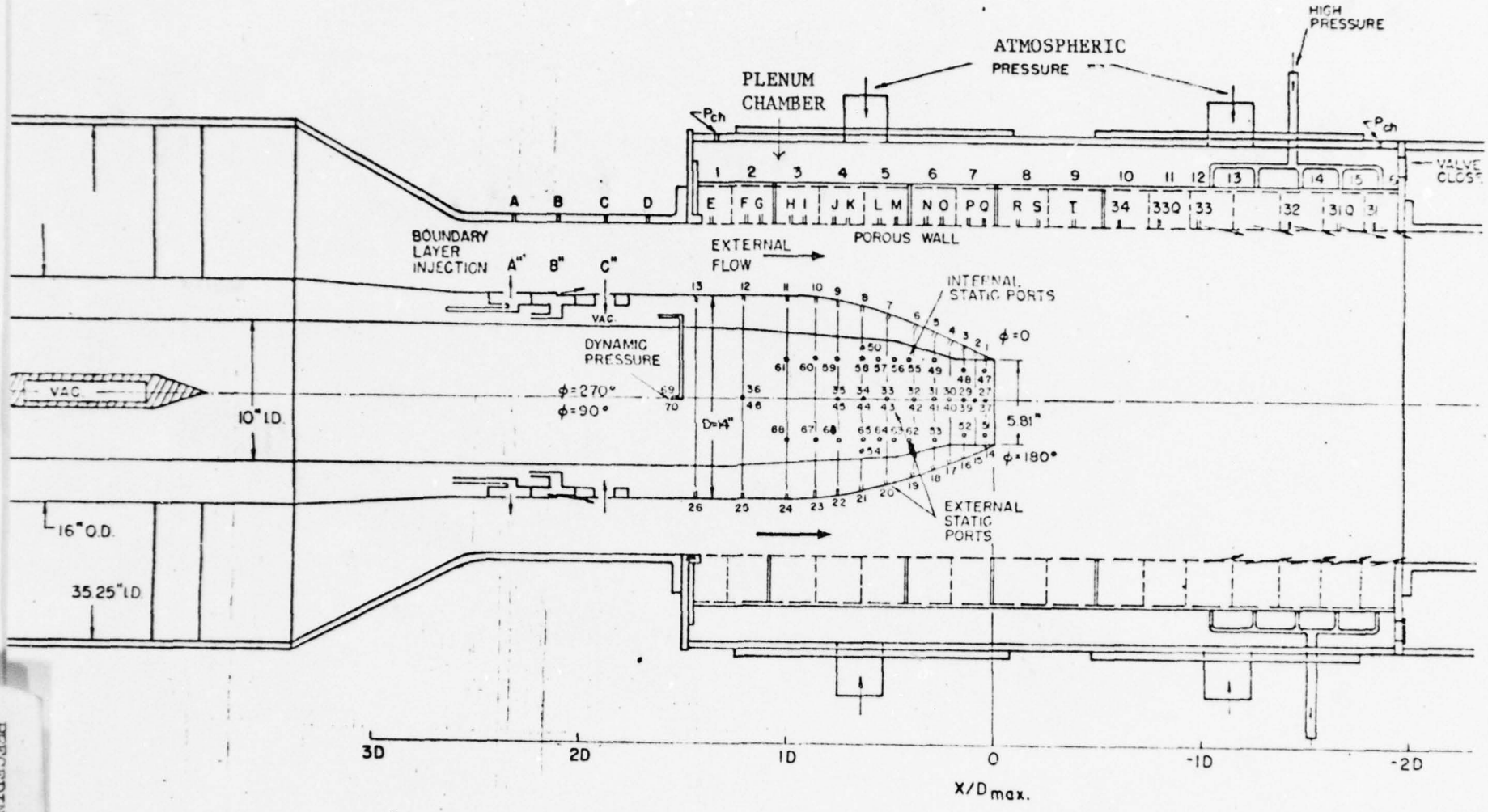

FIG. 2 SCHEMATIC OF FACILITY AND INSTRUMENTATION

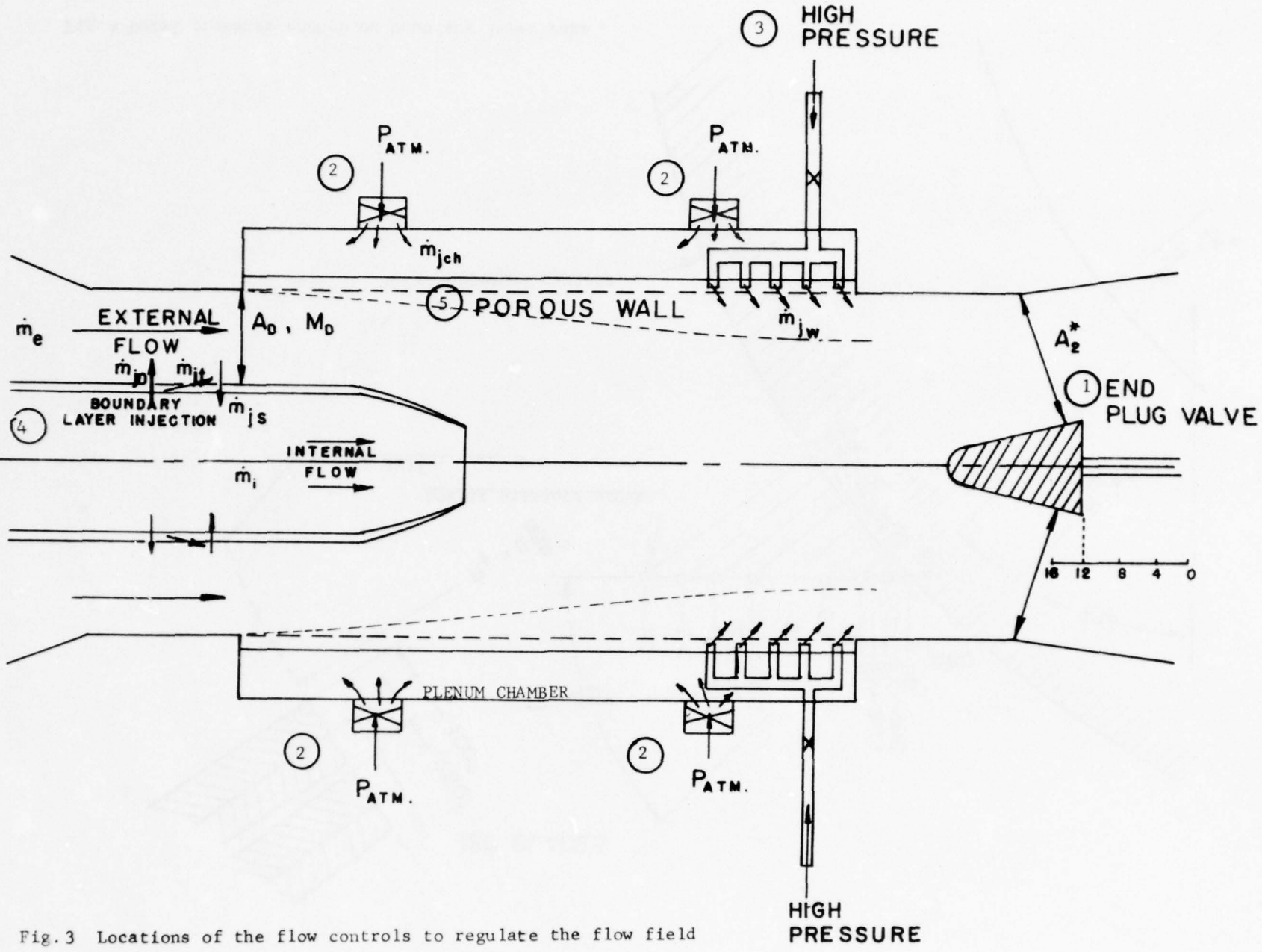

Fig. 3 Locations of the flow controls to regulate the flow field

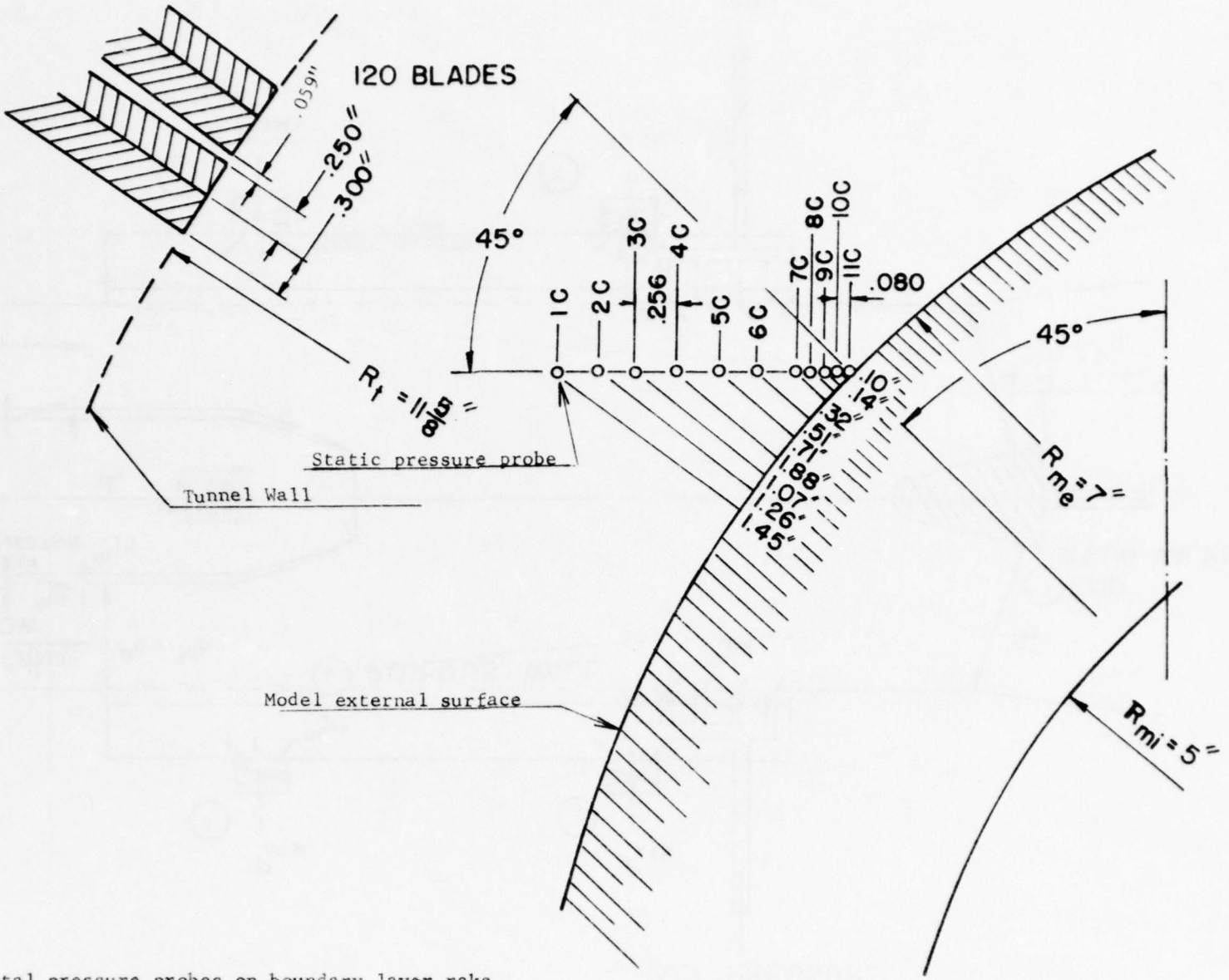

Fig.4 Total pressure probes on boundary layer rake

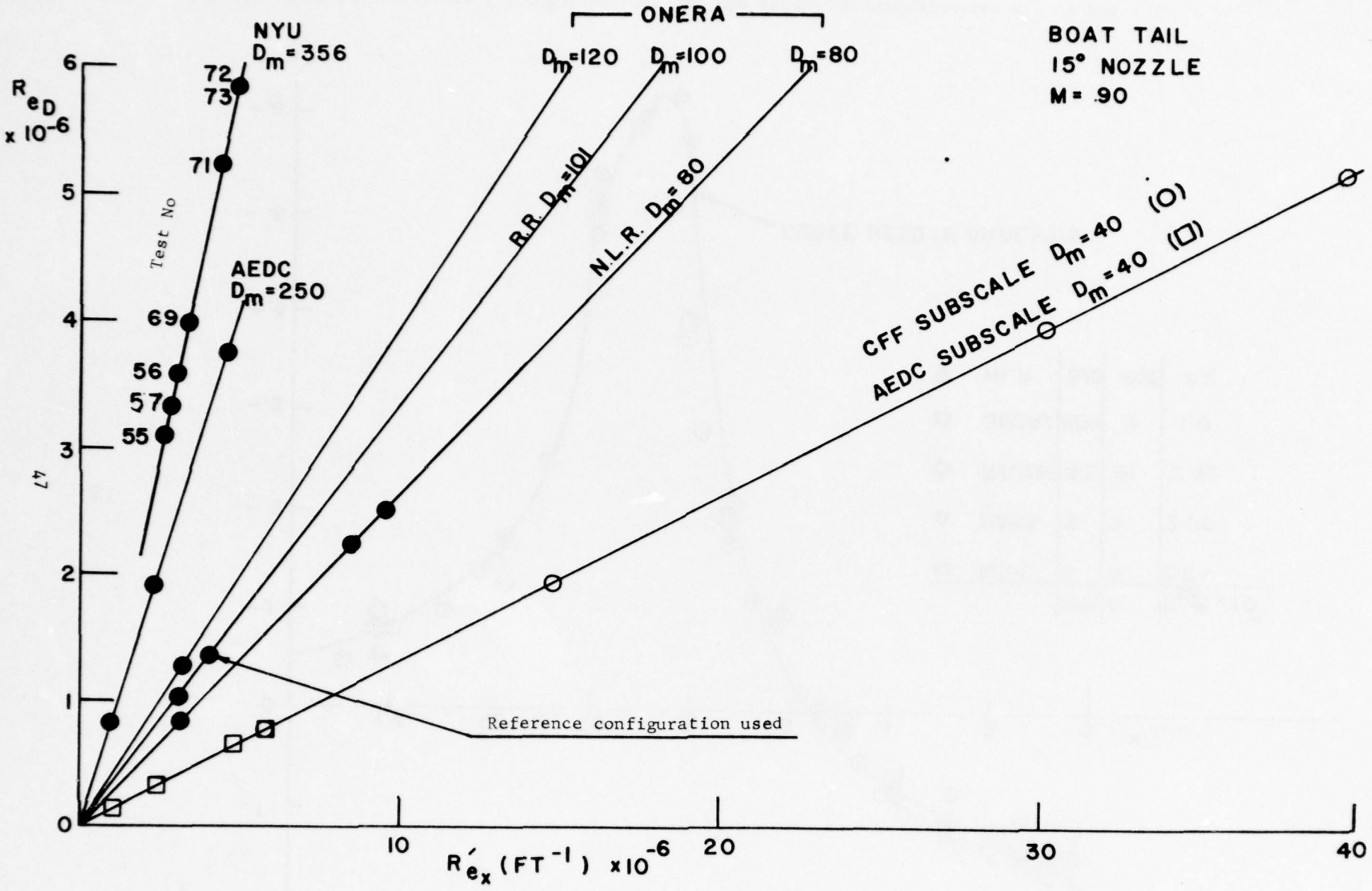

Fig. 5 R_{e_D} vs R'_{e_x} for various facilities, D_m = millimeters

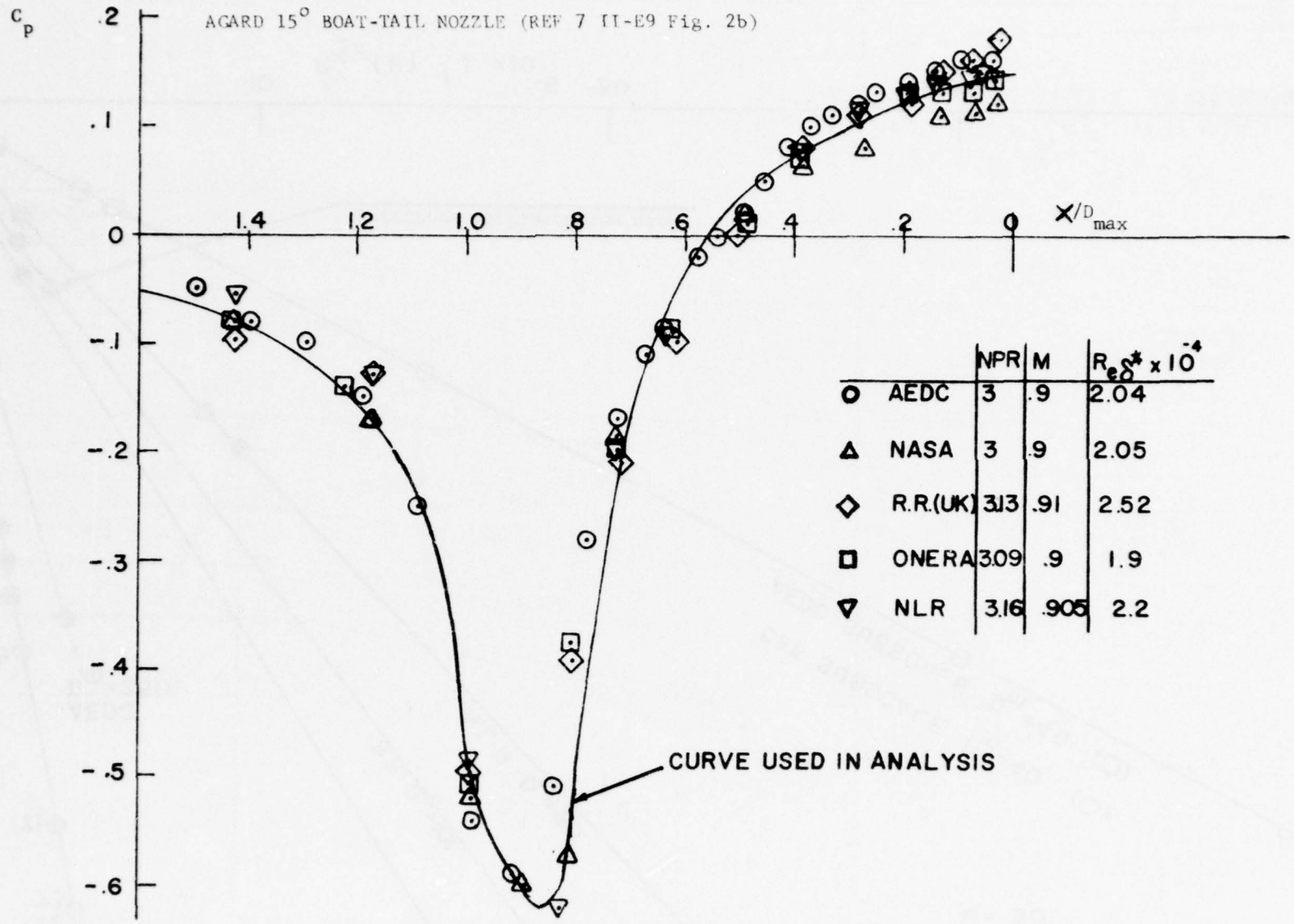

Fig. 6a Boat-tail pressure distribution used for the reference configuration M = .9 NPR = 3

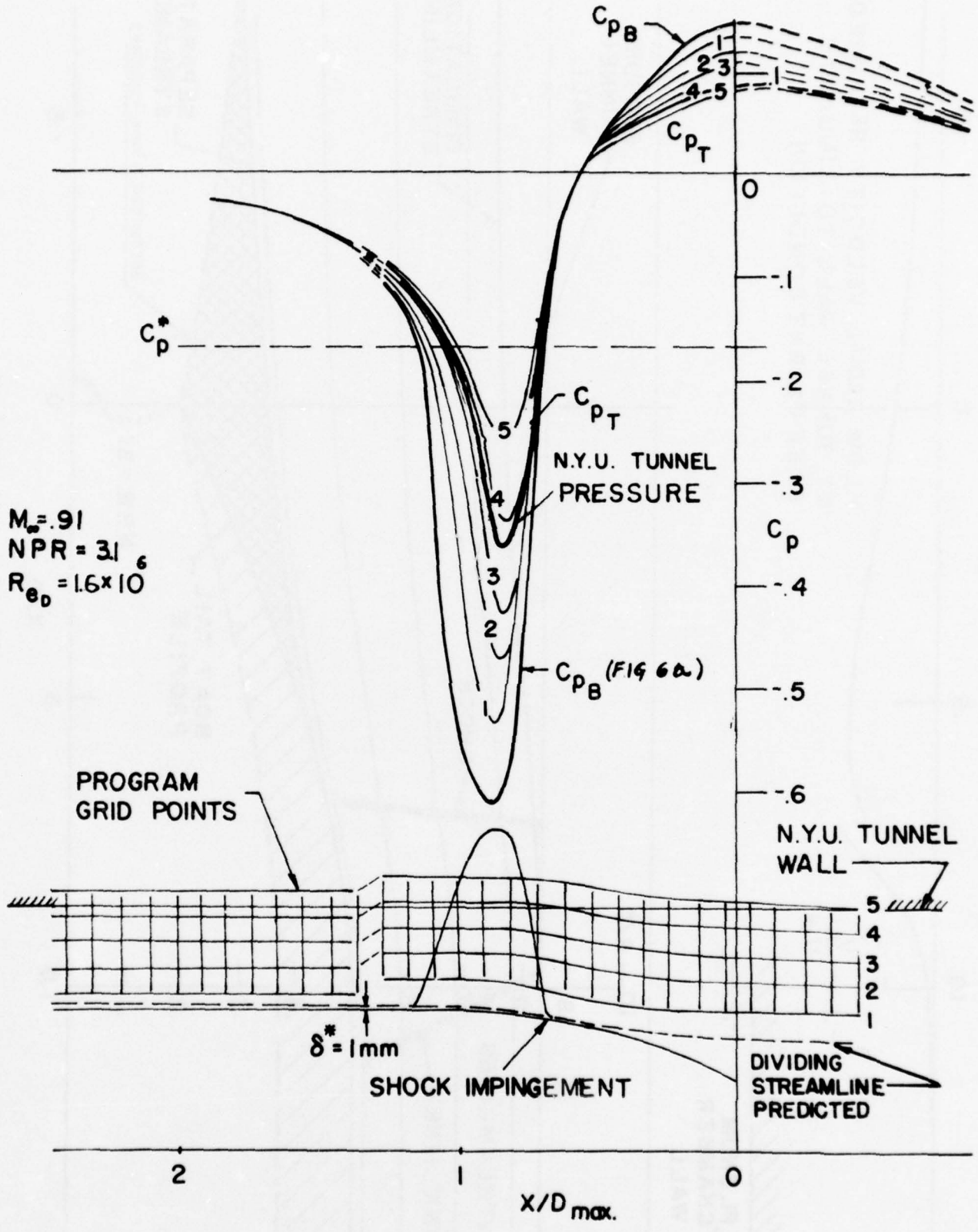

Fig.6b Computed pressure field from the given experimental pressure distribution at the body

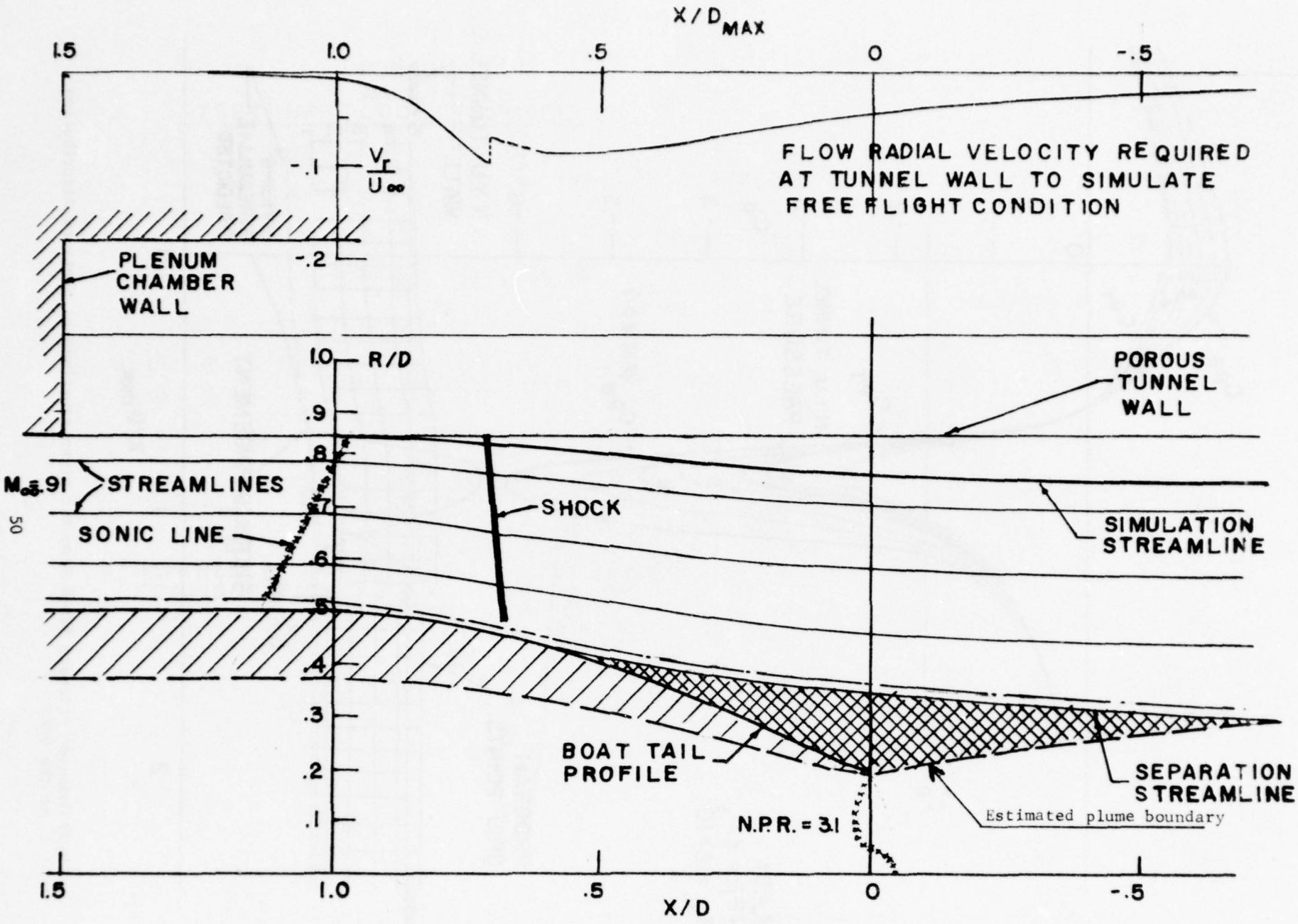

Fig. 6c Inviscid flow features of the reference configuration (semi-empirical)

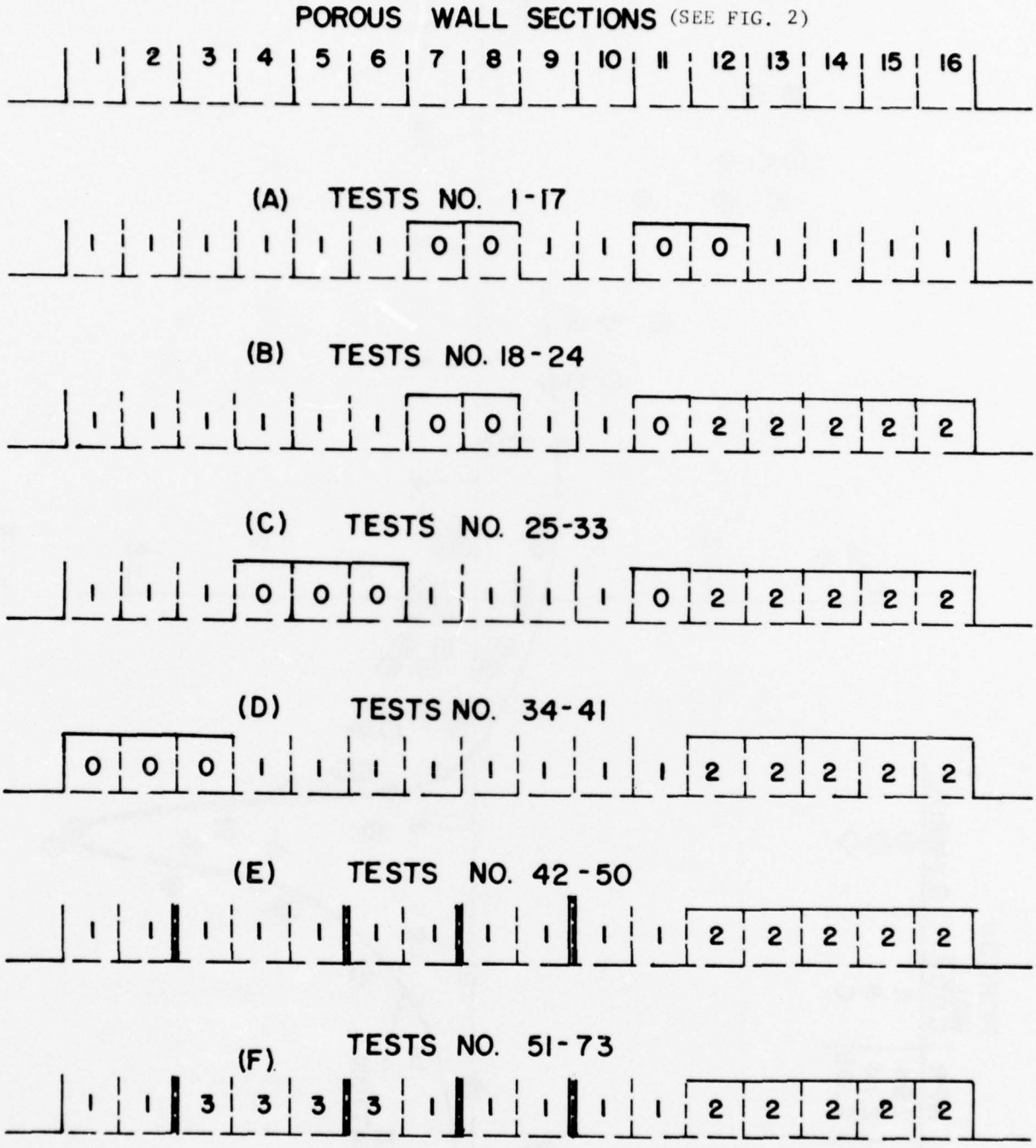

Fig. 7 Configurations of the porous wall

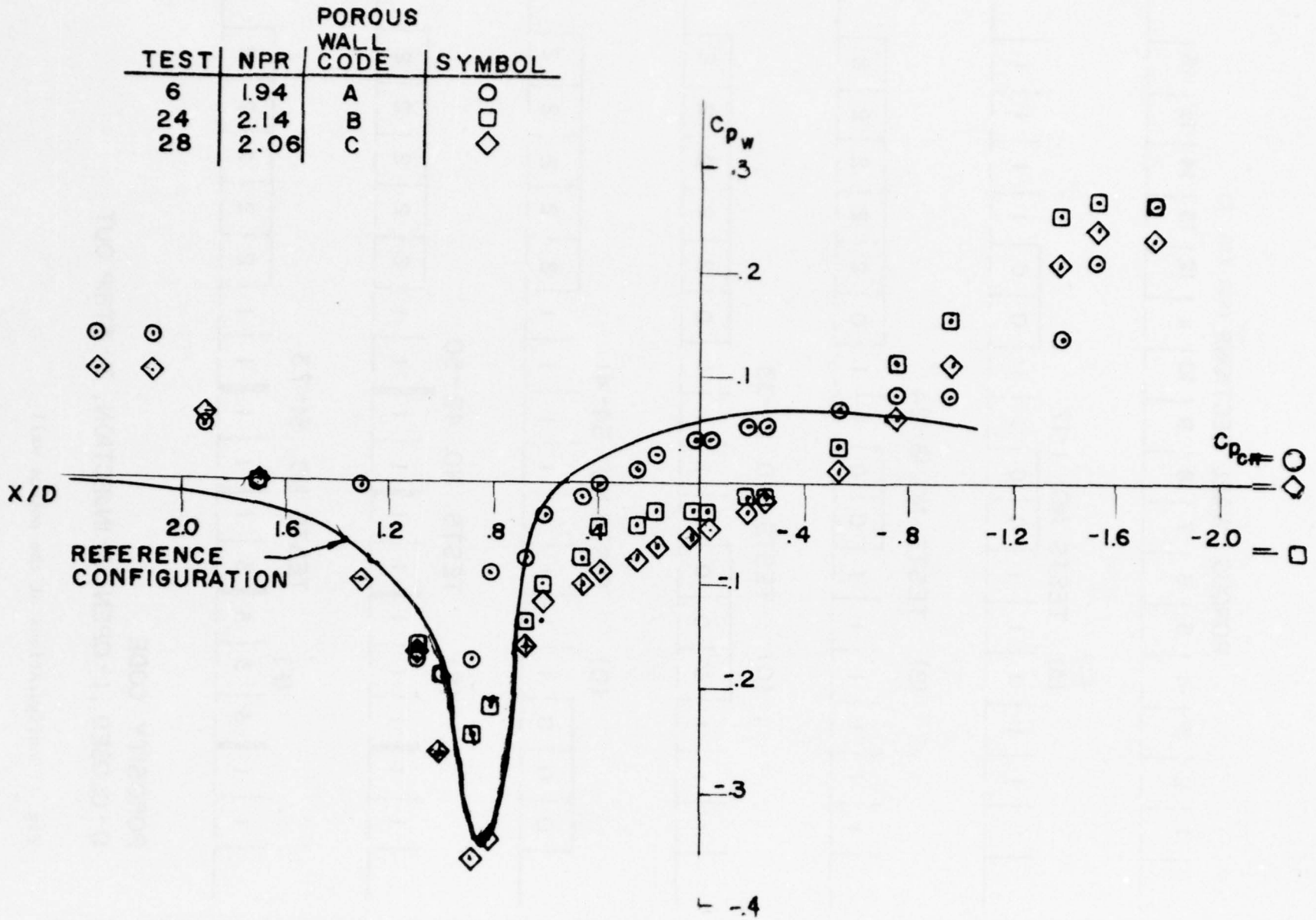

Fig. 8a Effect of porosity A,B,C, and porosity-injection code 2 on the tunnel wall pressure distribution

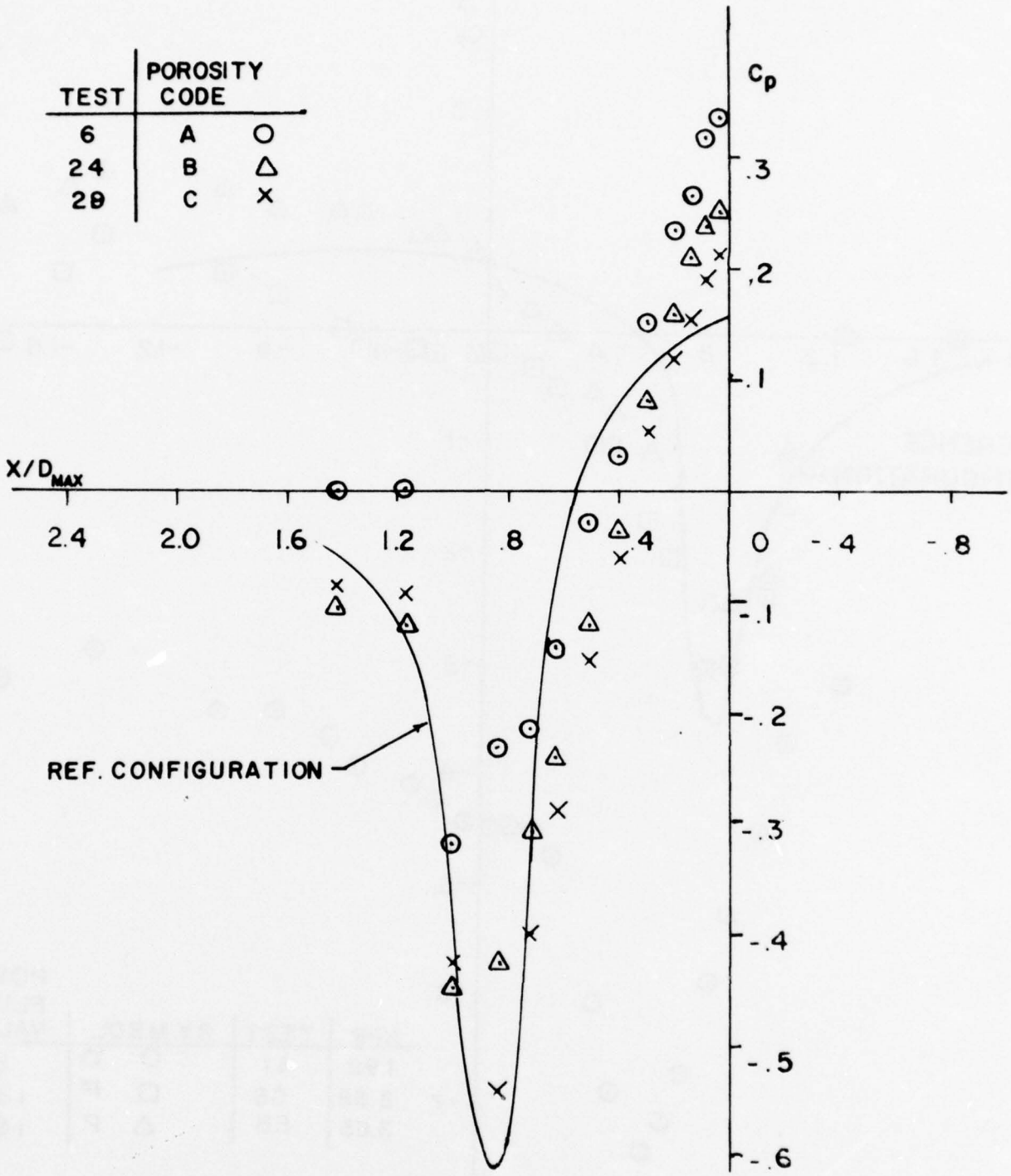

Fig. 8b Effect of porosity A,B,C on the boat-tail pressure distribution

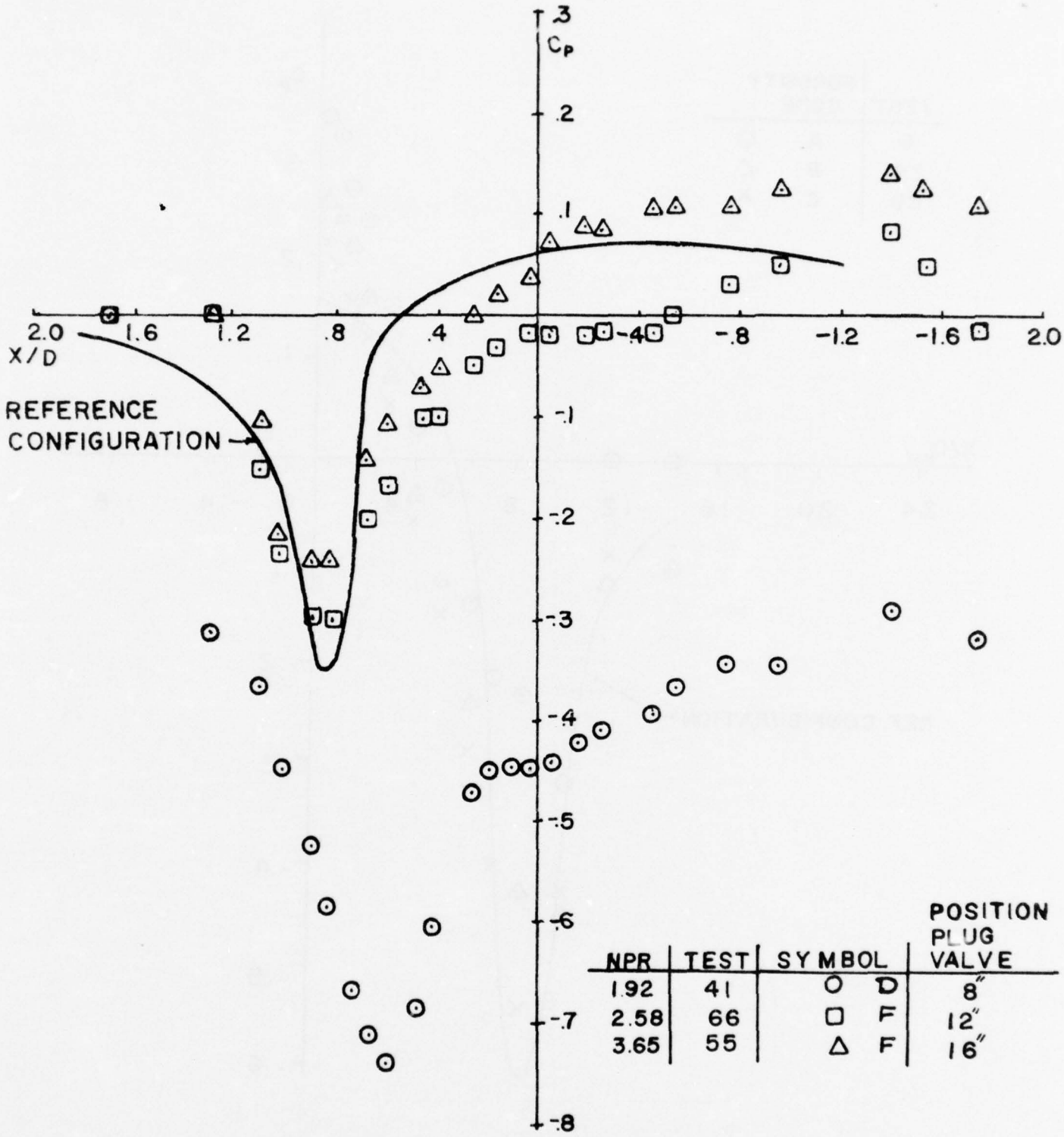

Fig. 8c Effect of plug valve position on tunnel wall pressure distribution

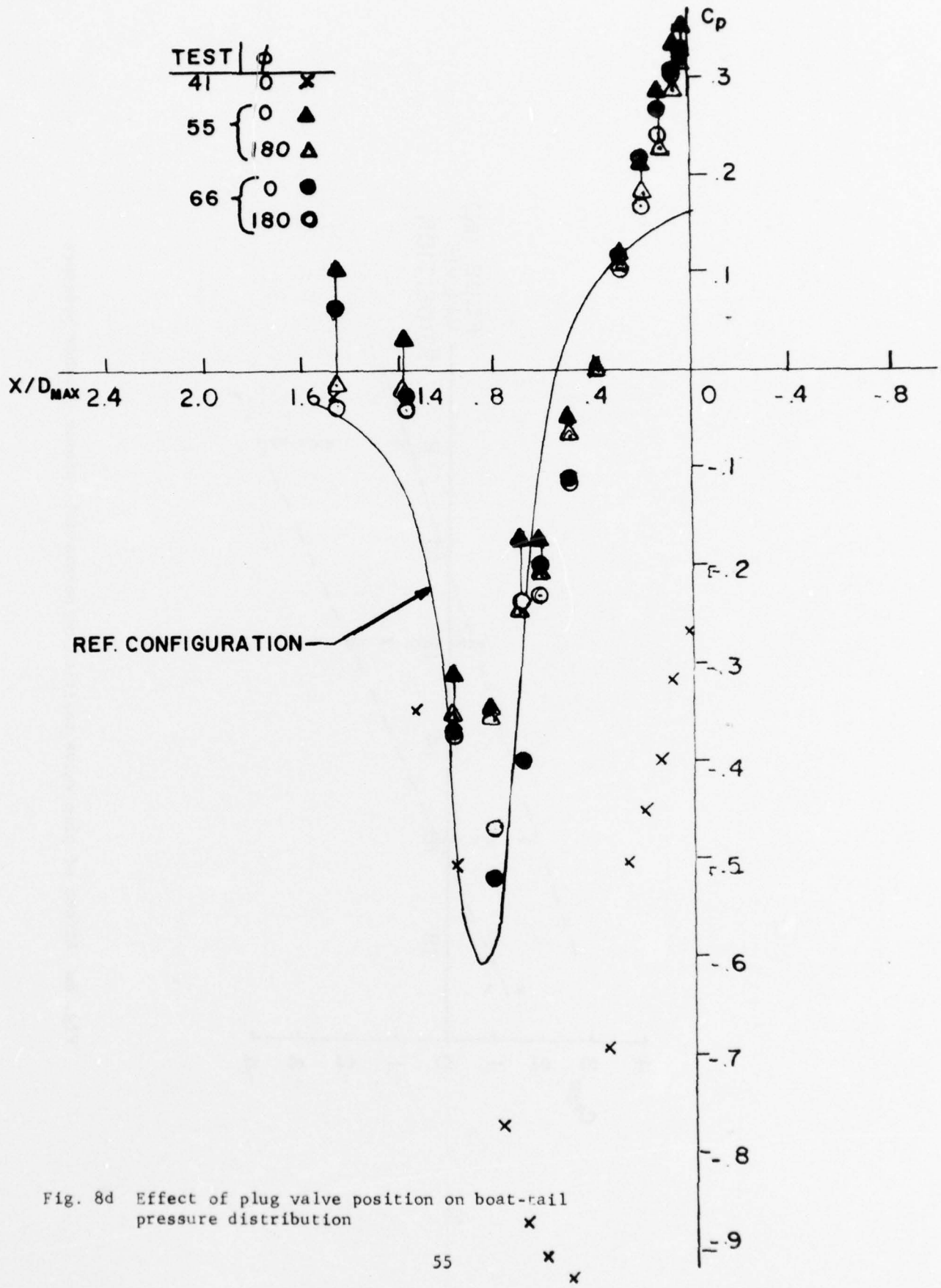

Fig. 8d Effect of plug valve position on boat-tail pressure distribution

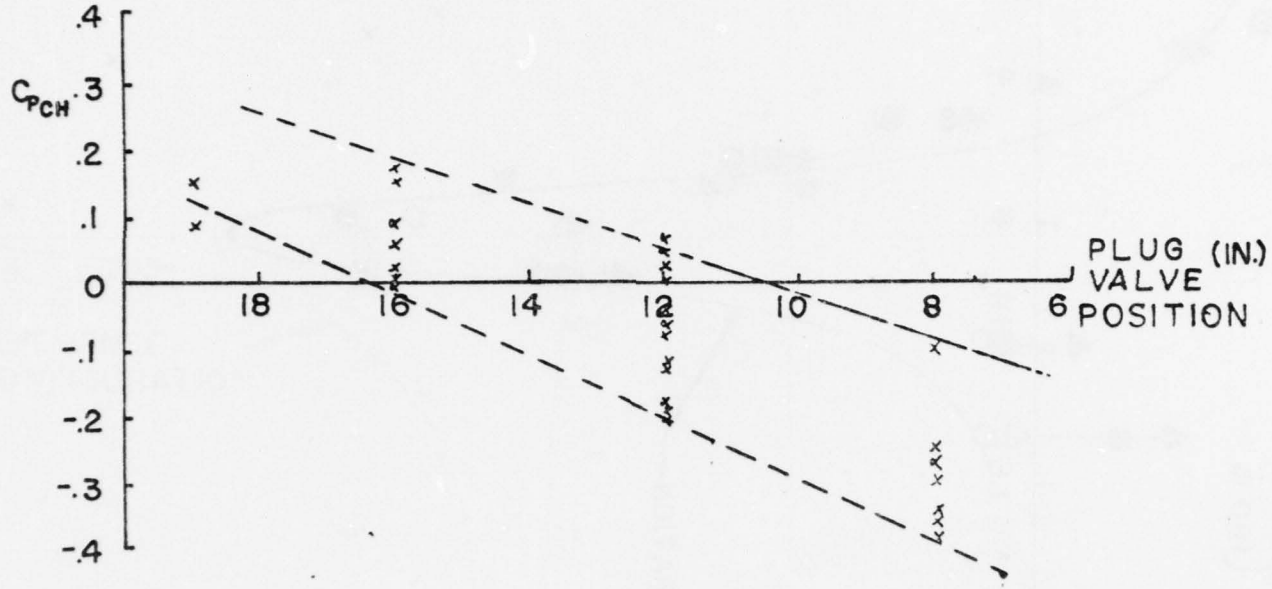

Fig. 8e Effect of plug valve position on porous wall plenum chamber pressure

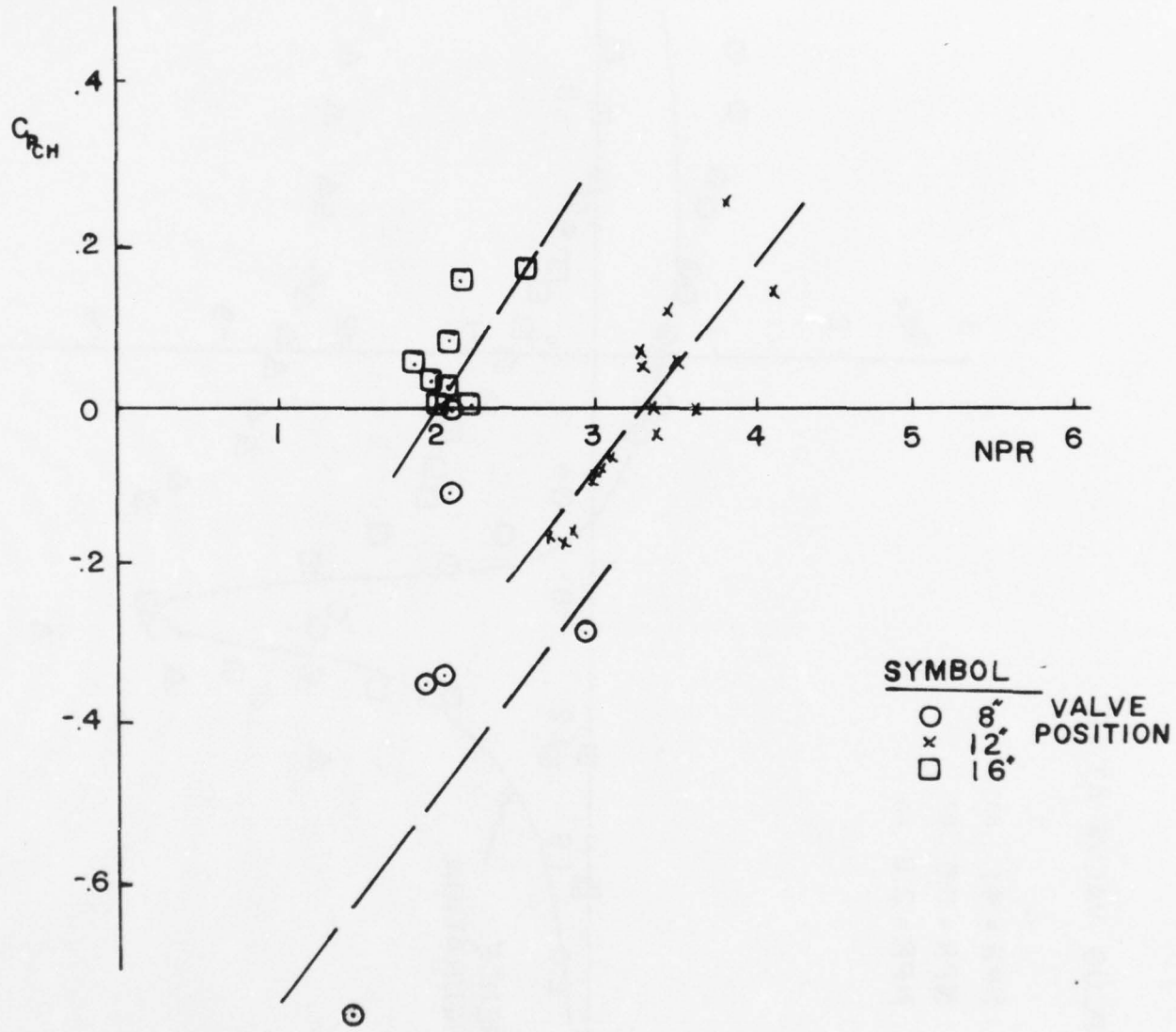

Fig. 8f Effect of NPR on porous wall chamber pressure

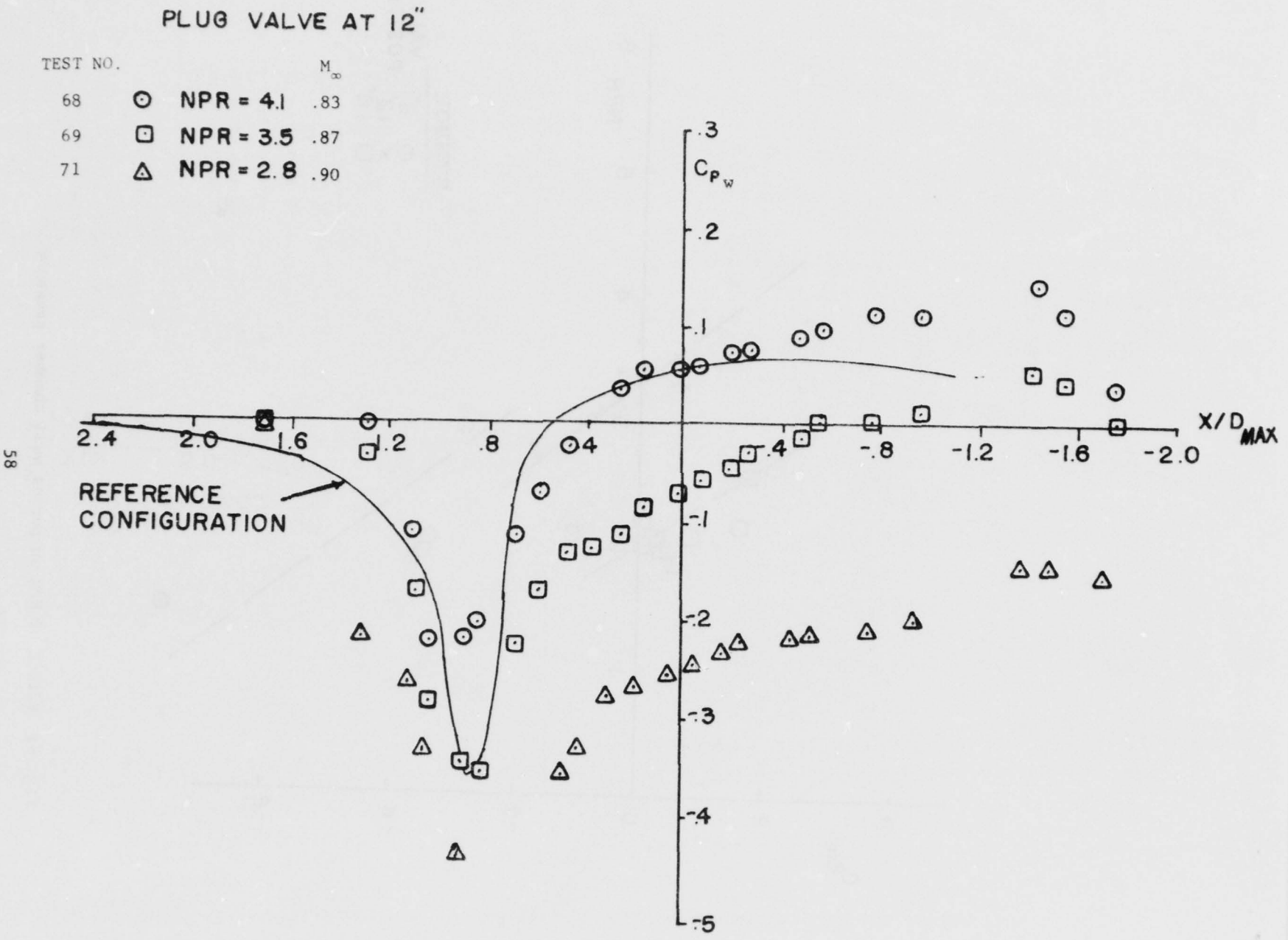

Fig. 8g Effect of NPR on wall pressure distribution

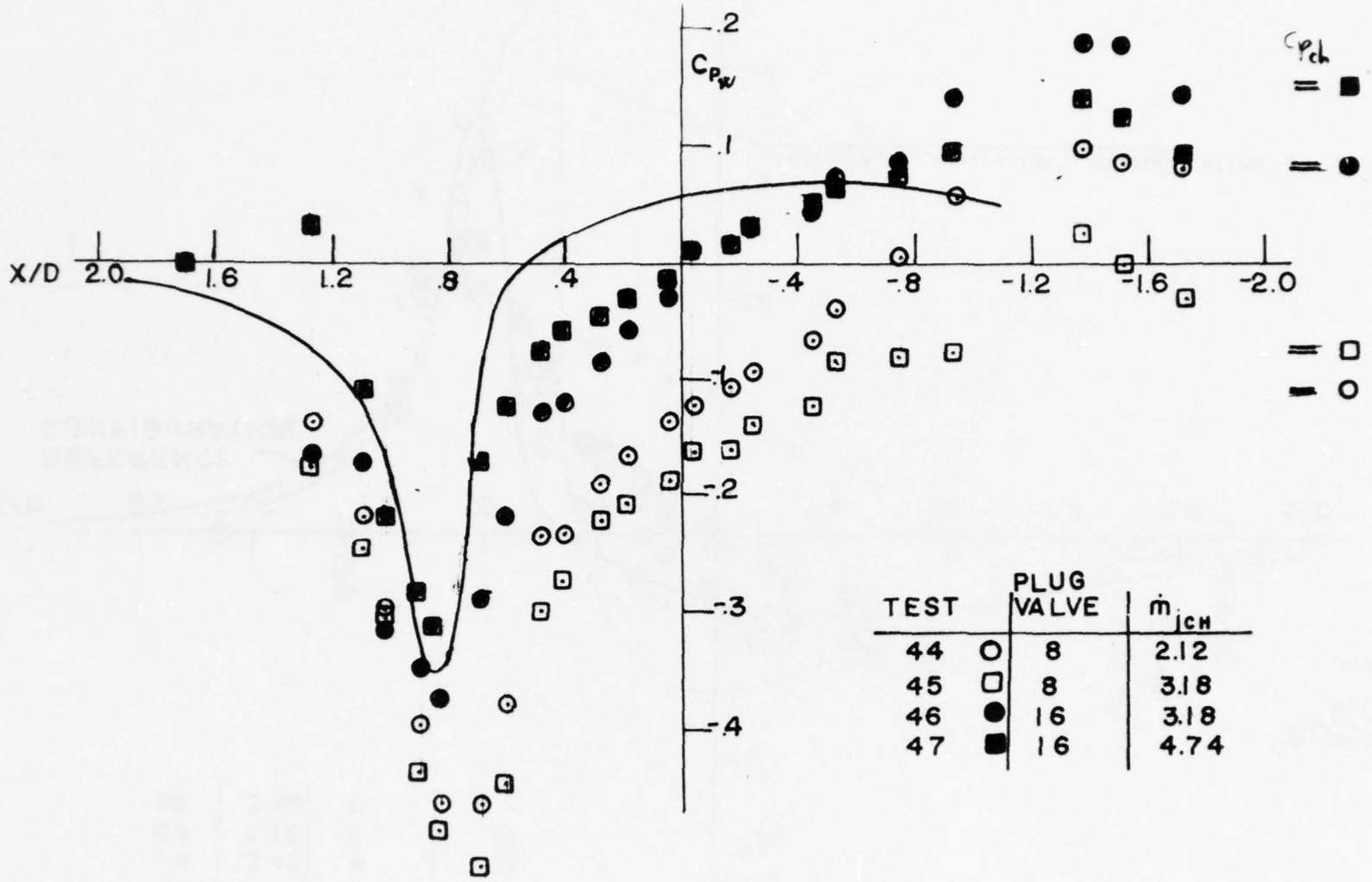

Fig. 8h Effect of injection in the plenum chamber of the porous wall for two different plug valve positions

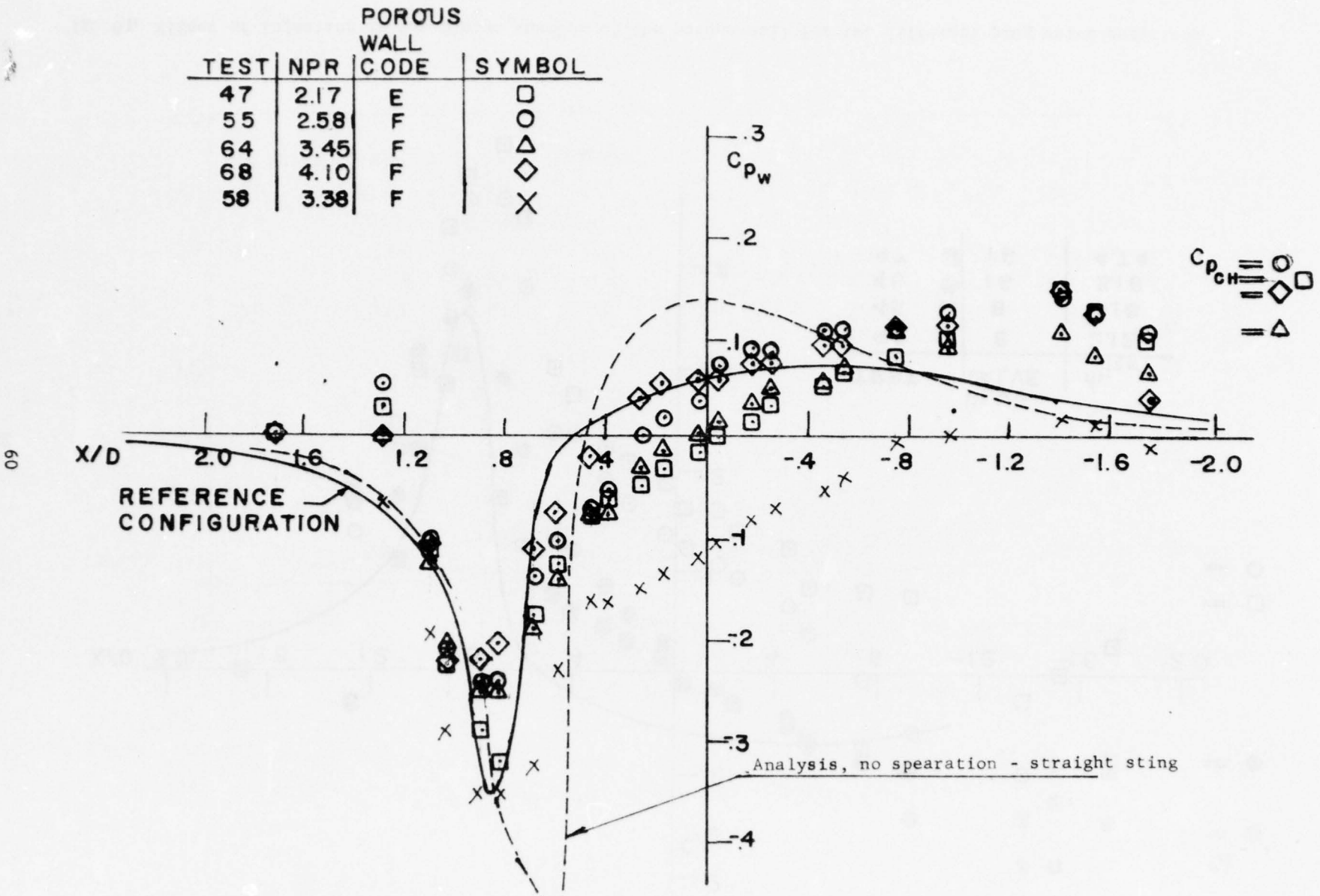

Fig. 9a Pressure distribution along the porous wall for reference configuration and several NPR

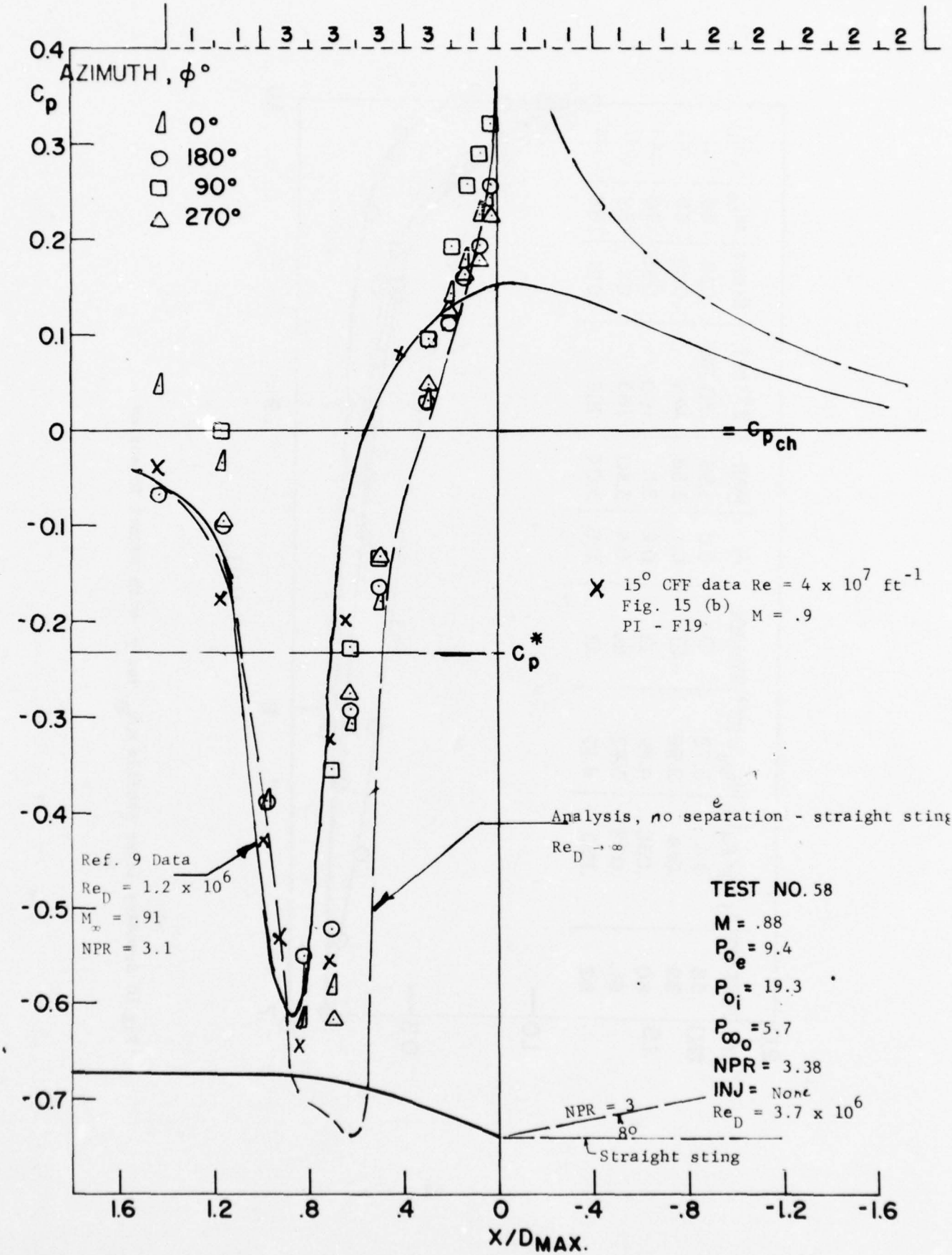

FIG. 9b C_p DISTRIBUTION ALONG THE BODY

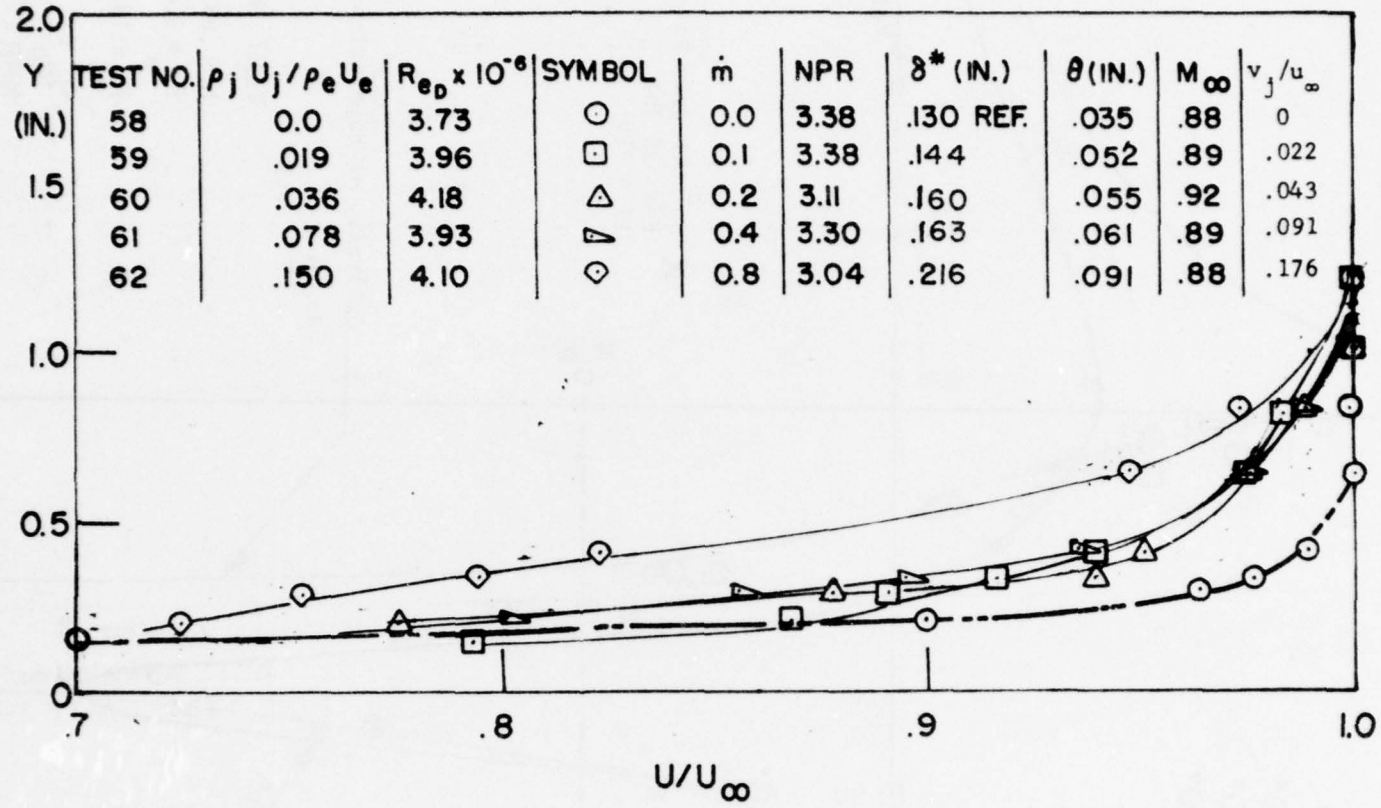

Fig.10 Boundary layer profile u/u_e vs. y with normal injection

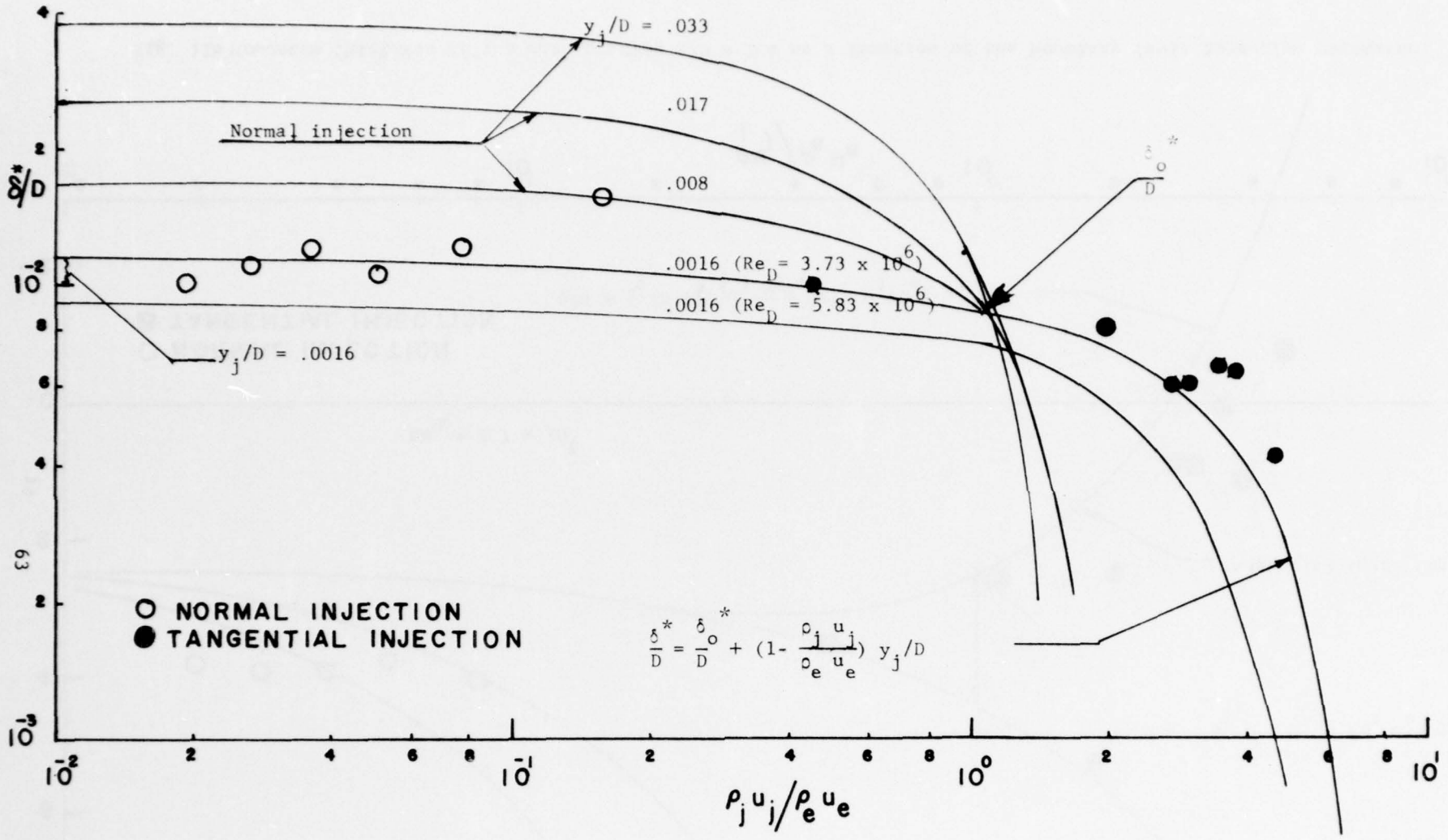

Fig. 11a Displacement thickness at the rake station x/D = 1.4 as a function of the boundary layer injection parameter,

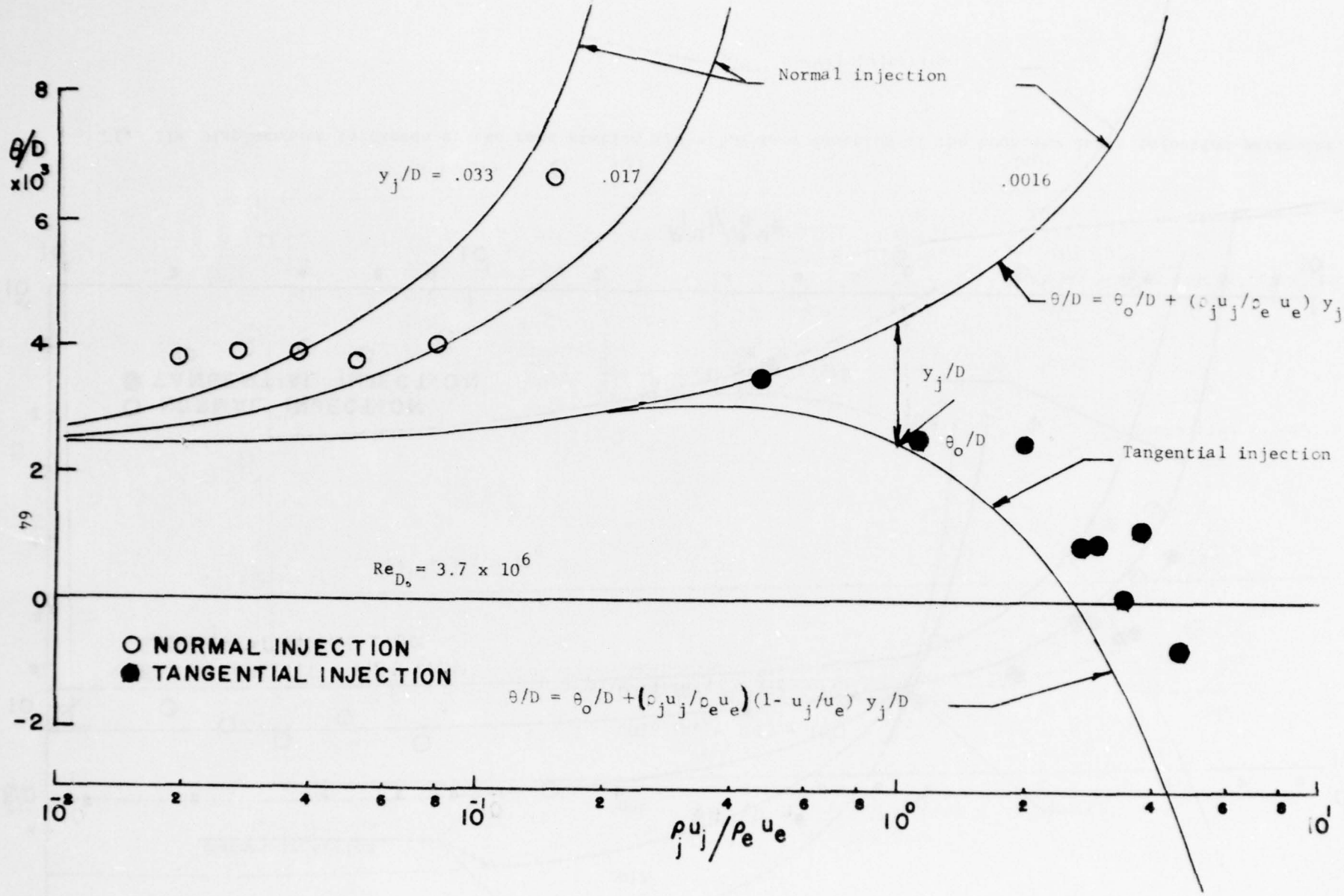

Fig. 11b Momentum thickness at the rake station x/D = 1.4 as a function of the boundary layer injection parameter.

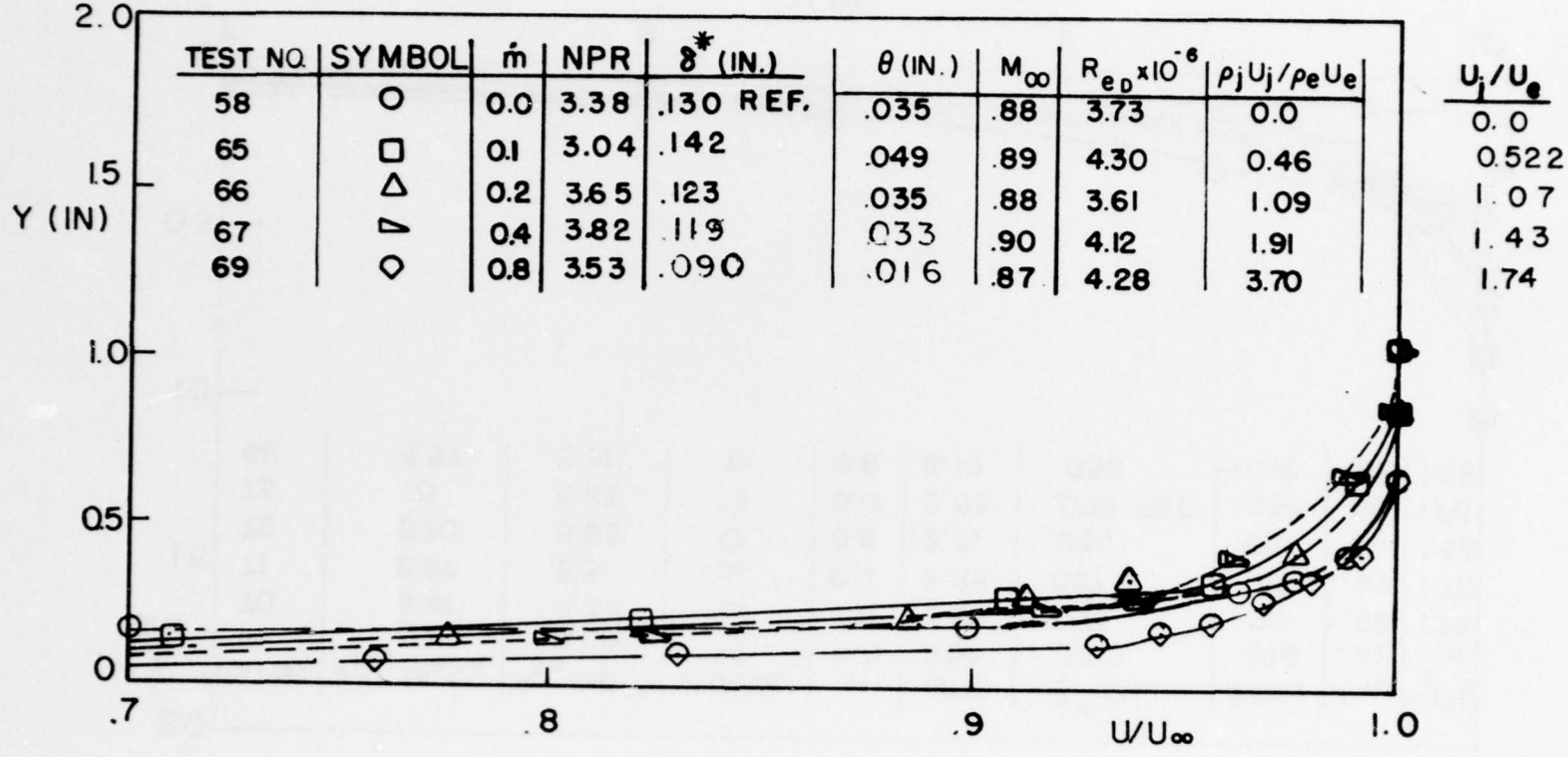

TEST NO.	SYMBOL	ṁ	NPR	δ* (IN.)	θ (IN.)	M∞	$R_{e_D} \times 10^{-6}$	$\rho_j U_j / \rho_e U_e$	U_j / U_e
58	○	0.0	3.38	.130 REF.	.035	.88	3.73	0.0	0.0
65	□	0.1	3.04	.142	.049	.89	4.30	0.46	0.522
66	△	0.2	3.65	.123	.035	.88	3.61	1.09	1.07
67	▷	0.4	3.82	.119	.033	.90	4.12	1.91	1.43
69	◇	0.8	3.53	.090	.016	.87	4.28	3.70	1.74

Fig.12 Boundary layer profiles u/u_e vs y with tangential injection $\dot{m}_{jt}$

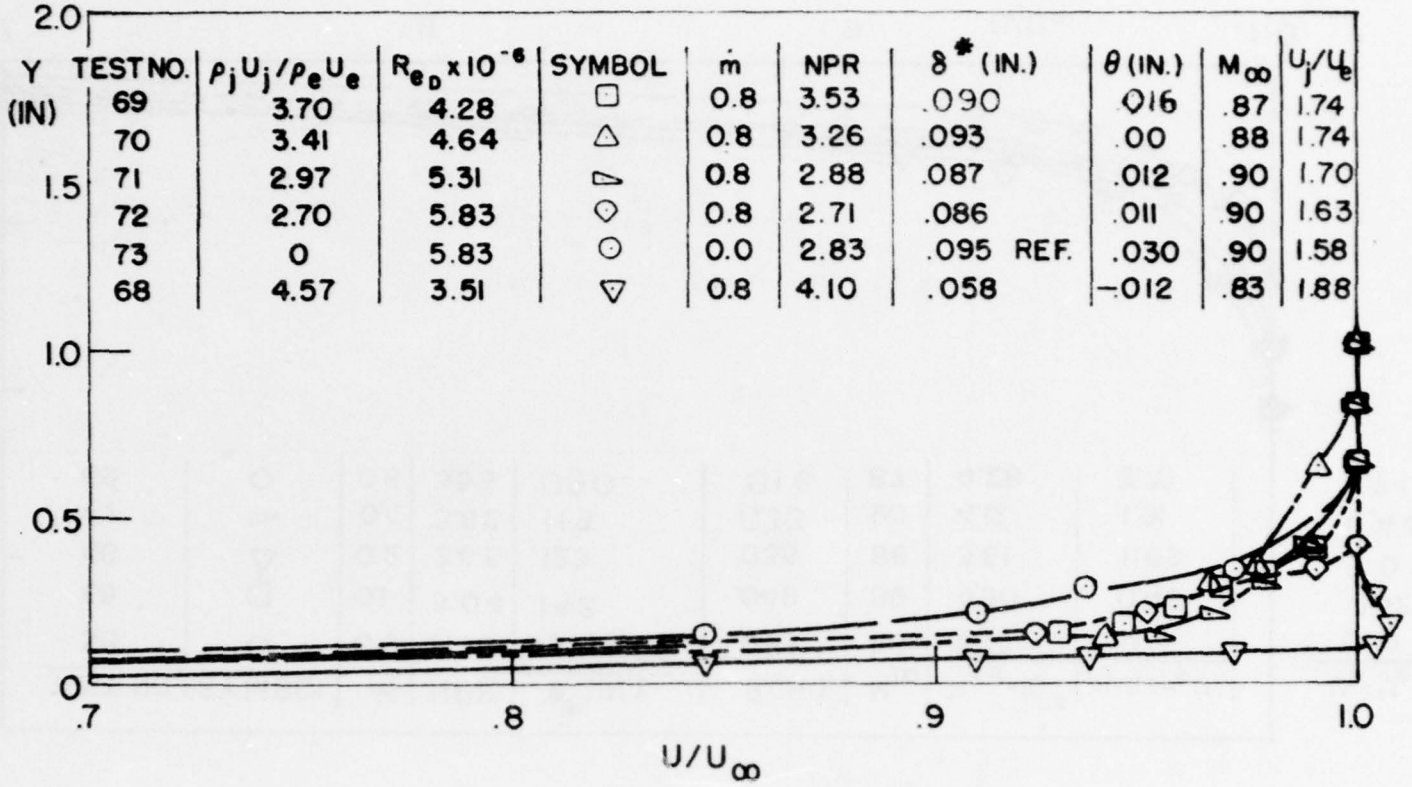

TEST NO.	$\rho_j U_j / \rho_e U_e$	$R_{e_D} \times 10^{-6}$	SYMBOL	$\dot{m}$	NPR	δ^* (IN.)	θ (IN.)	M_∞	U_j/U_e
69	3.70	4.28	□	0.8	3.53	.090	.016	.87	1.74
70	3.41	4.64	△	0.8	3.26	.093	.00	.88	1.74
71	2.97	5.31	▱	0.8	2.88	.087	.012	.90	1.70
72	2.70	5.83	◇	0.8	2.71	.086	.011	.90	1.63
73	0	5.83	⊙	0.0	2.83	.095 REF.	.030	.90	1.58
68	4.57	3.51	▽	0.8	4.10	.058	-.012	.83	1.88

Fig. 13 Boundary layer profile u/u_e vs. y with tangential injection $\dot{m}_{jt}$ lbm/sec constant

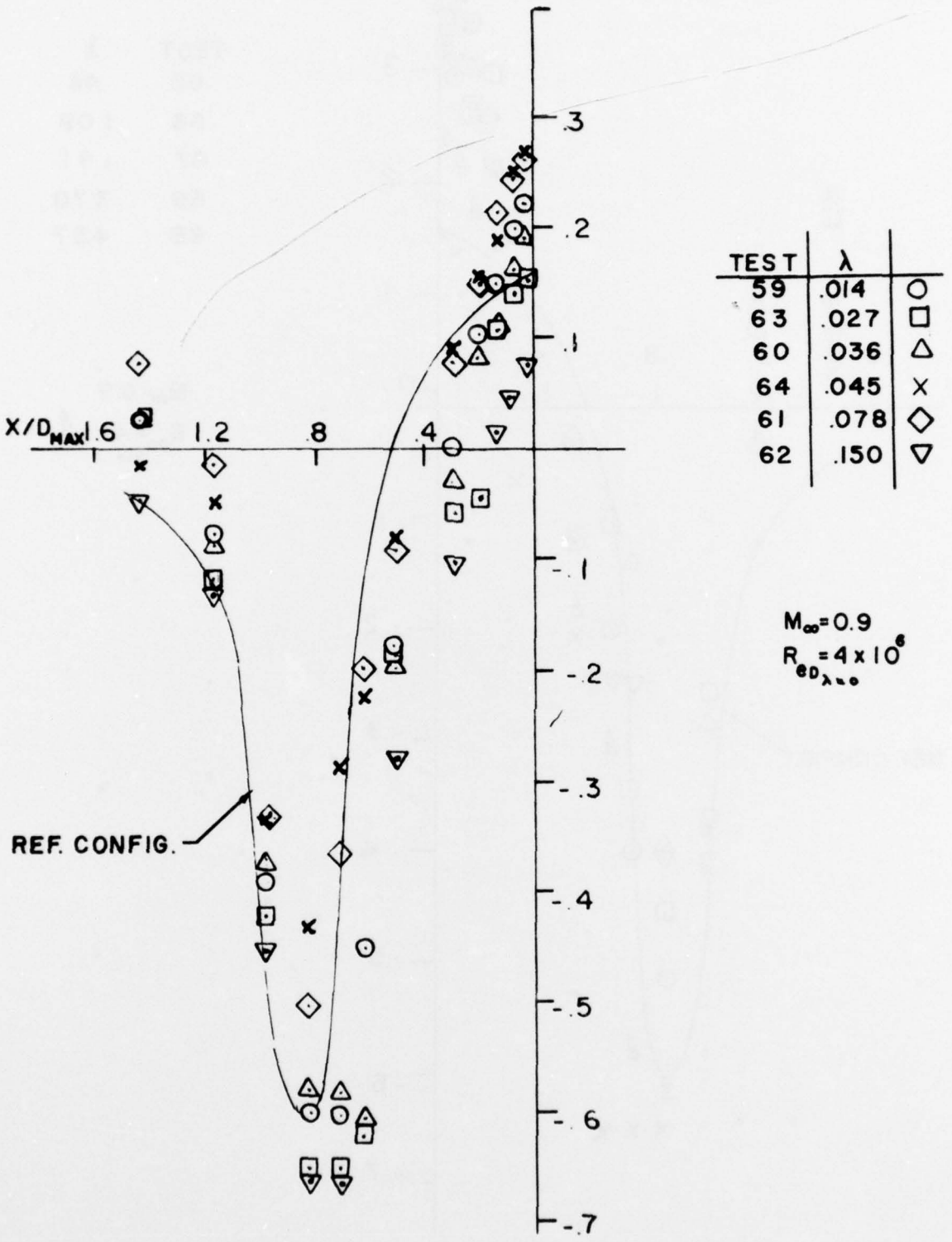

Fig. 14 Boat-tail pressure distribution ($\varphi = 0^{o}$) with different normal injection rates in the boat-tail boundary layer

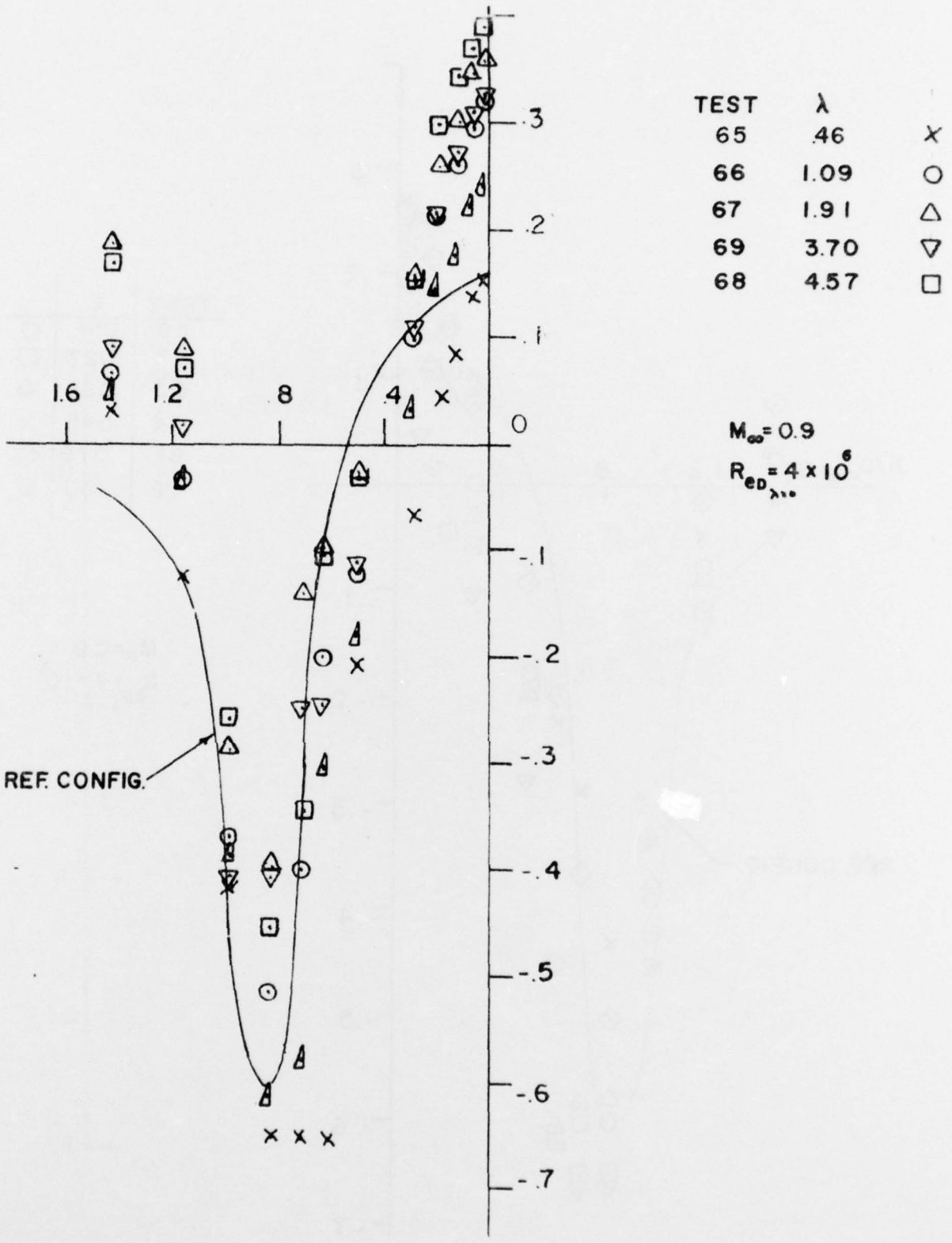

Fig. 15 Boat-tail pressure distribution ($\omega = 0^\circ$) with different tangential injection rates in the boat-tail boundary layer

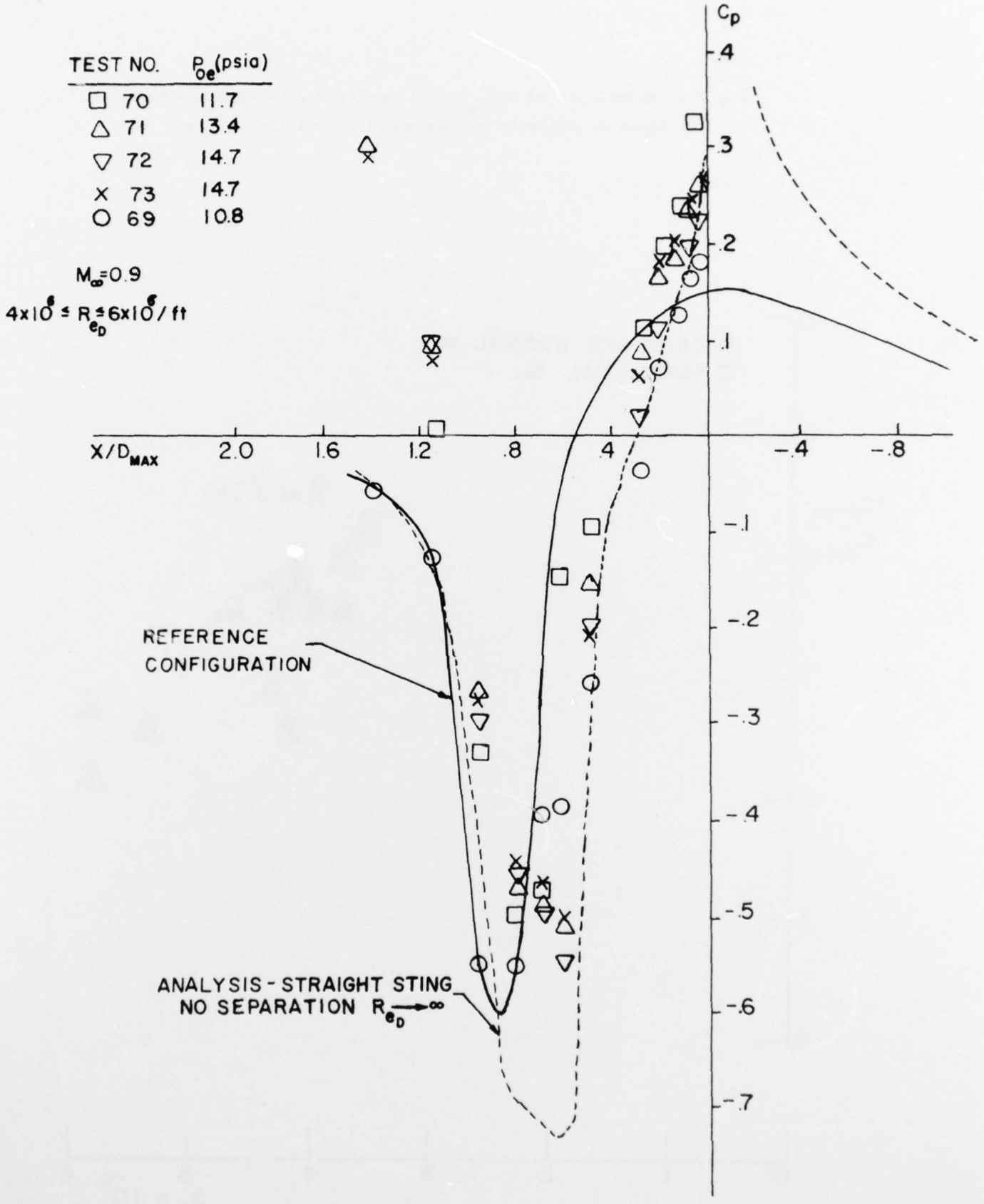

Fig. 16 Boat-tail pressure distribution with different external flow stagnation pressures and fixed internal flow and injection flow rates

Fig 17a Correlation of Cp_{min} point location with Reynolds number based on diameter of the model for various δ^* (in)

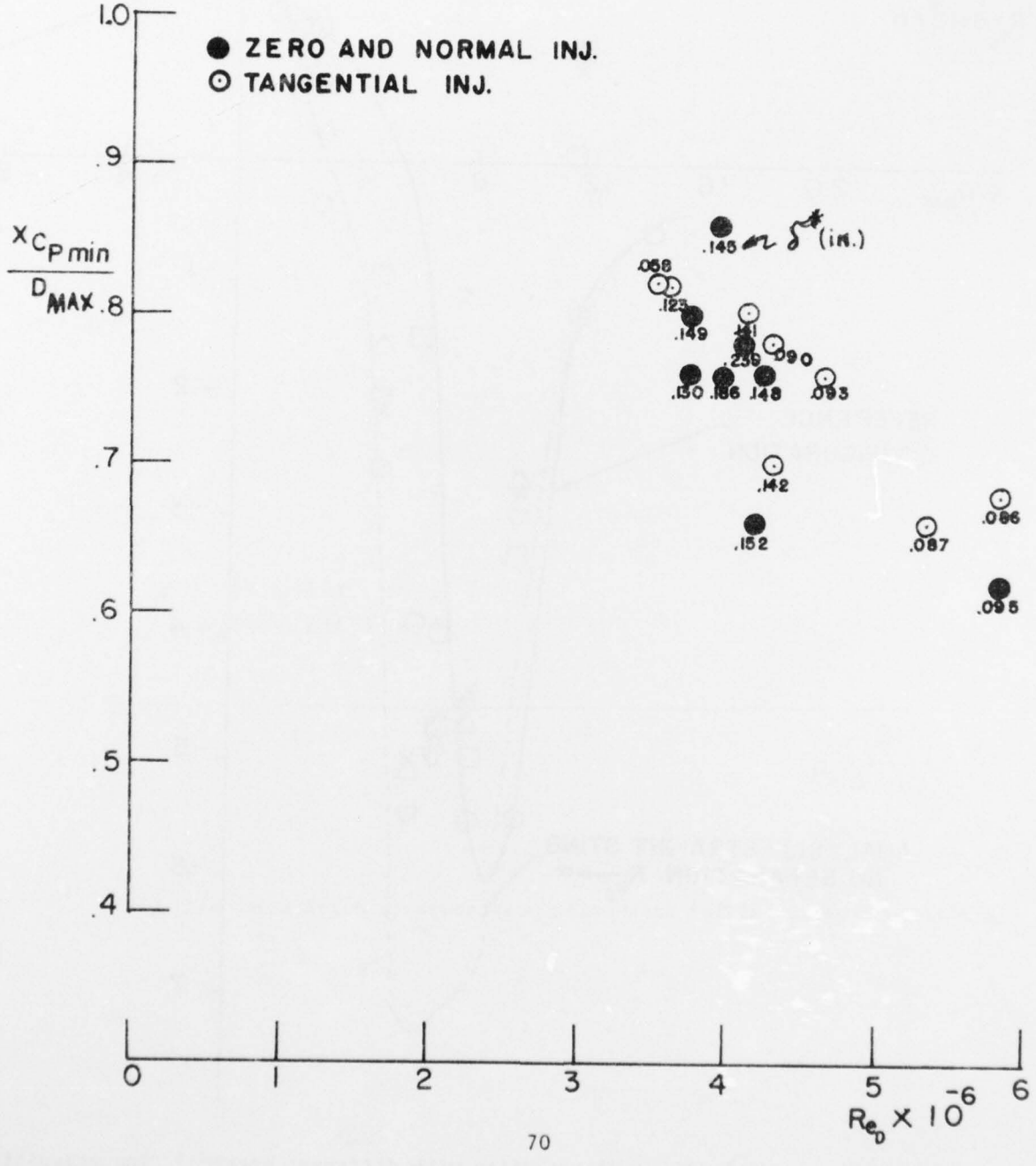

Fig 17b Correlation of Cp_{min} point location with NPR for various Normal (N) and Tangential (T) injection $\dot{m}$ lbm/sec

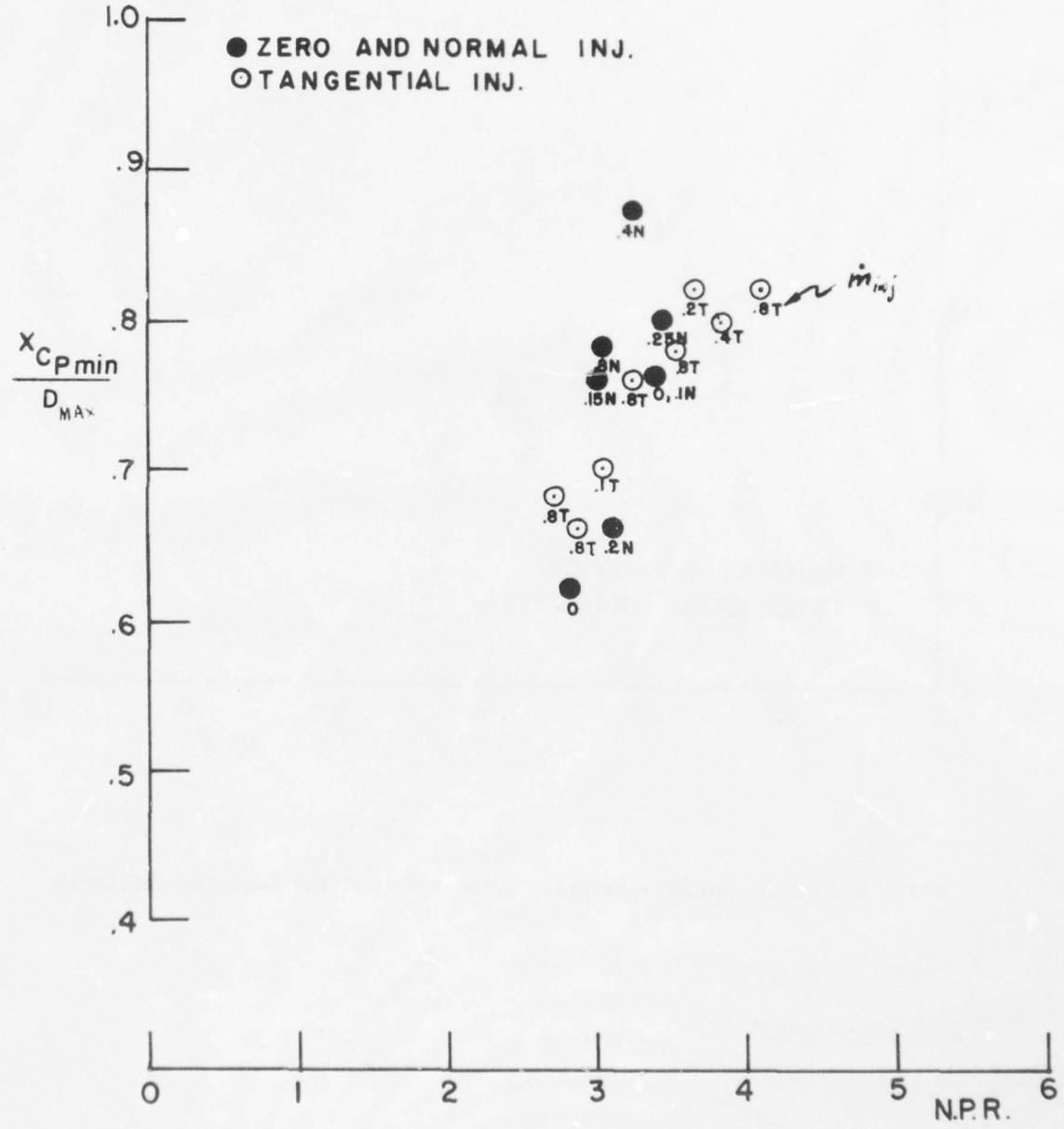

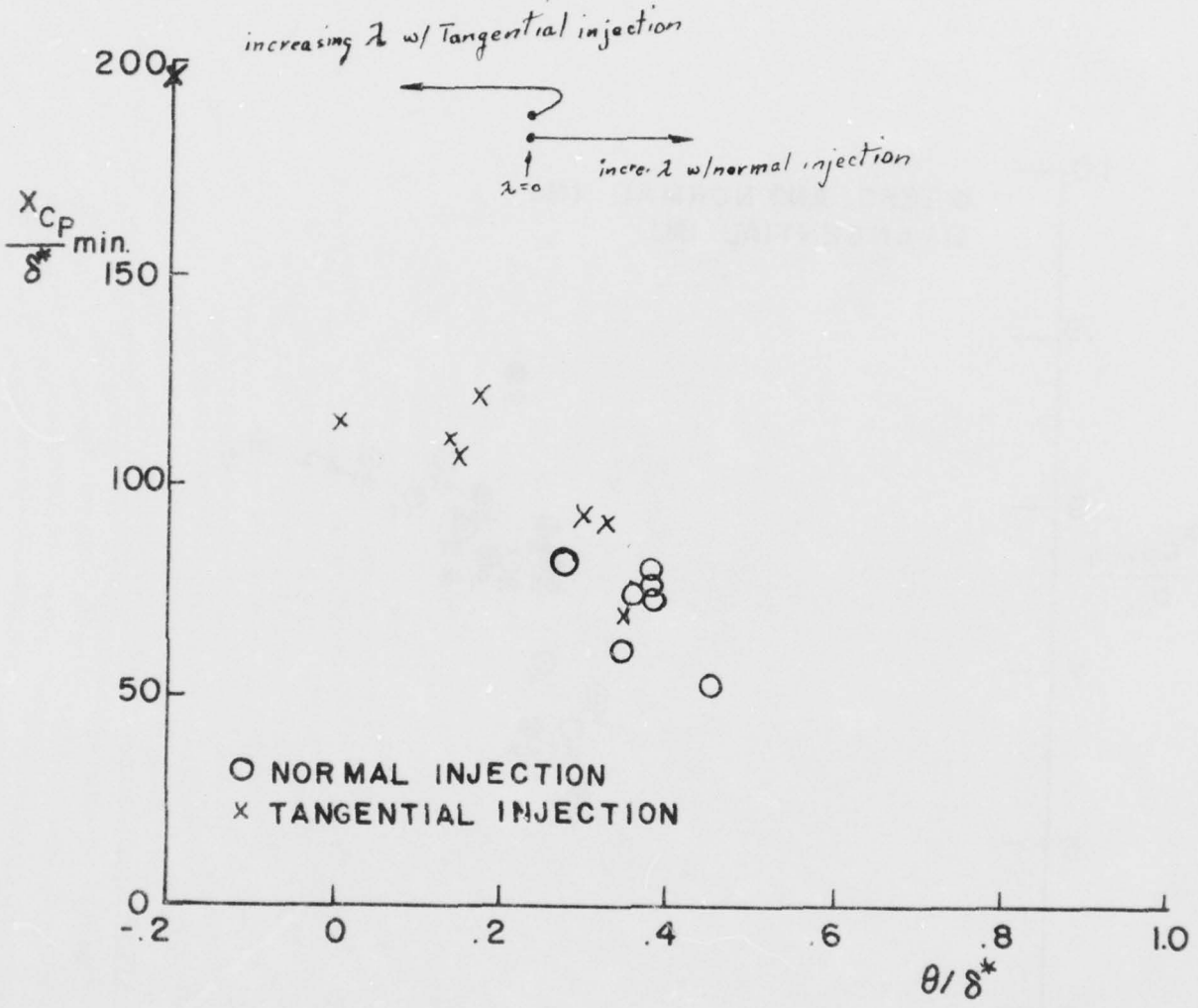

Fig. 17c Correlation of separation point with initial momentum thickness

Fig 18a Correlation of Cp^* point location with Reynolds number based on diameter of the model for various δ^* (in)

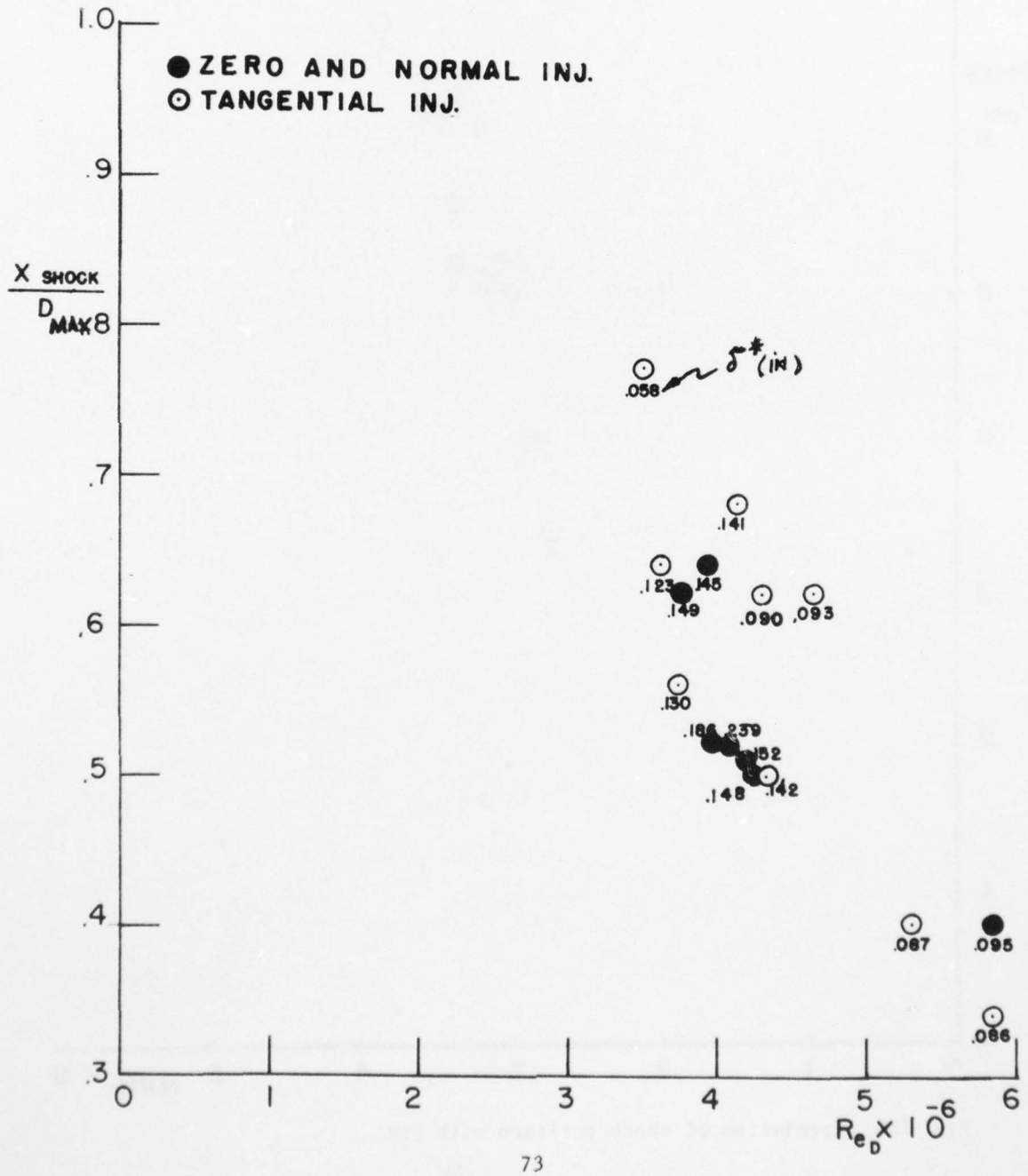

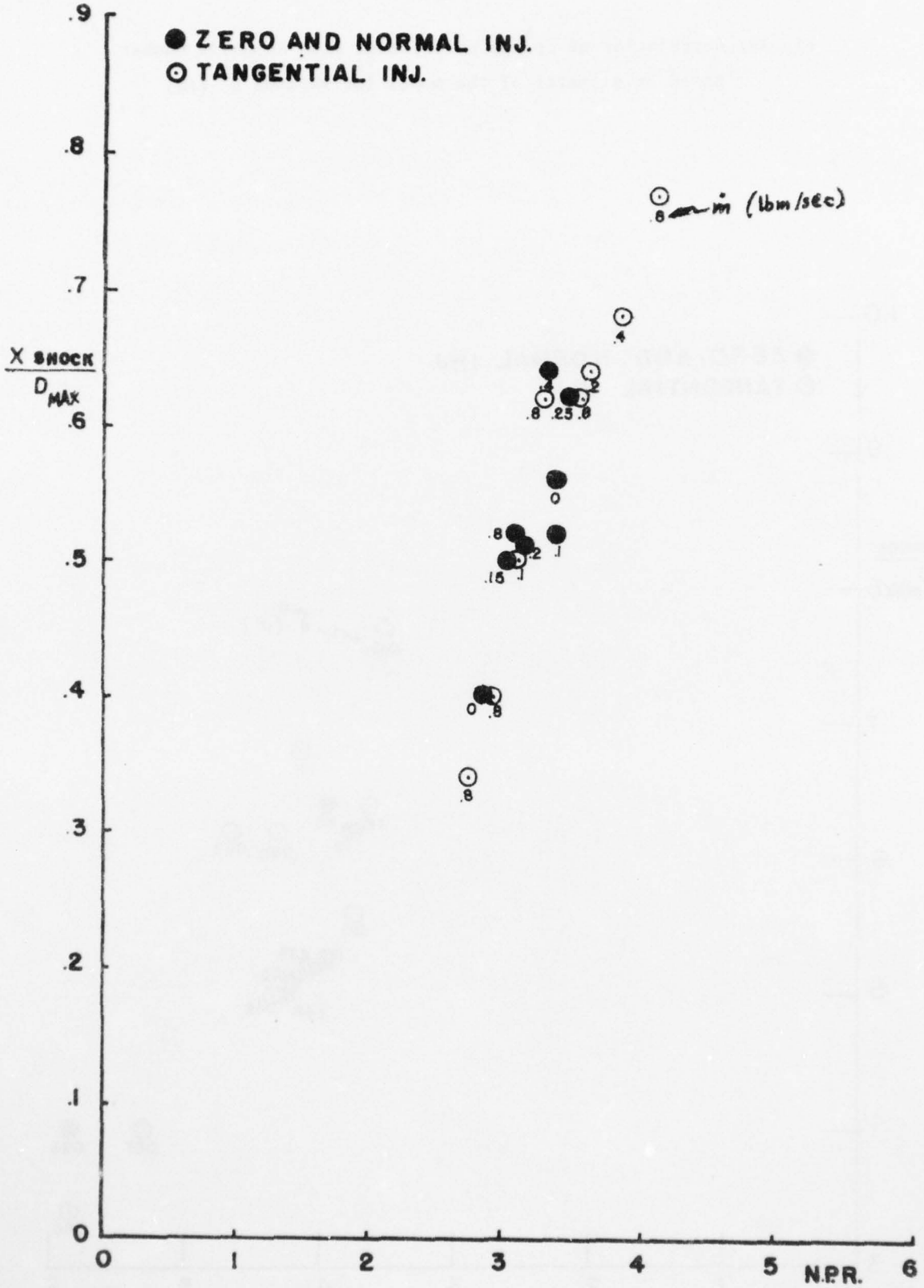

Fig. 18b Correlation of shock position with NPR

REFERENCES

1. Panunzio, S., "Investigation of Boundary Layer Shock Interaction at Transonic Speed," Final Report WPAFB ARL 74-0114, July 1974.

2. Roffe, G. and Miller, G., "Similarity Parameters and Their Sensitivity for Transonic Airframe Exhaust Nozzle Interactions," Advanced Technology Laboratories, Inc., ATL TR 175, July 1972.

3. Grossman, B. and Melnik, R.E., "The Numerical Computation of the Transonic Flow Over Afterbodies Including the Effect of Jet-Plume and Viscous Interactions," AIAA Paper No. 75-62, AIAA 13th Aerospace Sciences Meeting, January 1975.

4. Presz, E. Grund, W., Jr. and Konarski, M., "Predicting Airframe/ Exhaust Nozzle Interactions at Transonic Mach Numbers," AIAA Paper No. 71-720, AIAA/SAE 7th Propulsion Joint Specialists Conference, June 1971.

5. Presz, W.M., Jr., and Pitkins, E.T., "An Analytical Model of Axisymmetric Afterbody Flow Separation," AIAA Paper No. 75-65, AIAA 13th Aerospace Sciences Meeting, June 1975.

6. Calarese, W., "Analysis of Transonic Viscous-Inviscid Interactions on Axisymmetric Afterbodies with Jet Effects and Boattail Injection in Separated Regions," Final Report WPAFB FDL-TR-75-117, September, 1975.

7. Ferri, A., "Improved Nozzle Testing Techniques in Transonic Flow," AGARDograph No. AGARD-AG-208, October 1975.

8. Wang, H.C. and Srokowski, A., "Flowfield Determination for Axially Symmetric Configurations at Transonic Speeds," New York University (USA) Report NYU-AA-73-11, June 1973.

9. Deer, D.J., "Results of Tests on Single Afterbody Nozzles Defined by AGARD," Rolls Royce Ltd., England, pp. 67, March 1974.

10. Ferri, A., Elzweig, S., and Baronti, P., "Numerical Solution of Transonic Flows about Quasi-Cylindrical Configurations," Advanced Technology Labs., Inc. Westbury, New York, AIAA Journal, Vol. 12, No. 10, p. 1447-1448, October 1974.

11. Reubush, D.E., "The Effect of Reynolds Number on Boat-tail Drag," NASA Langley Research Center, Hampton, Va., AIAA Paper No. 75-63, AIAA 13th Aerospace Sciences Meeting, January 20-22, 1975


FILM
4